

THESIS

HYDROGEOLOGIC CHARACTERIZATION OF AN ALPINE GLACIAL TILL,
SNOWY RANGE, WYOMING

Submitted by

Tyler B. Houghton

Department of Geosciences

In partial fulfillment of the requirements

For the Degree of Master of Science

Colorado State University

Fort Collins, Colorado

Fall 2011

Master's Committee:

Advisor: Michael Ronayne

John Stednick
William Sanford

ABSTRACT

HYDROGEOLOGIC CHARACTERIZATION OF AN ALPINE GLACIAL TILL, SNOWY RANGE, WYOMING

Characterization of sediment hydraulic properties is essential to understanding groundwater movement. In many mountain watersheds, surficial geologic material, such as glacial till, plays an important role in water and nutrient chemical cycling. Hydraulic properties of alpine glacial tills are infrequently measured, requiring efforts to characterize this complex geologic material. This research involved the use of multiple measurement techniques to determine the saturated hydraulic conductivity of surficial glacial tills at the Glacier Lakes Ecosystem Experiments Site (GLEES) in south-central Wyoming.

During the summer of 2010, three *in situ* methods (double-ring infiltrometer, mini disk infiltrometer, and Guelph permeameter) were used to measure field-saturated hydraulic conductivity (K_{sat}) at 32 locations around GLEES. Estimated K_{sat} values obtained with the double-ring infiltrometer had a geometric mean of 0.12 cm/min and range of 0.007 to 0.40 cm/min. The Guelph permeameter had a geometric mean of 0.094 cm/min and range of 0.003 cm/min to 0.776 cm/min, and the mini disk infiltrometer obtained estimates with a geometric mean of 0.014 cm/min and ranged from 0.002 cm/min to 0.043 cm/min. The double-ring infiltrometer and Guelph permeameter

measure K_{sat} at a physical scale that is large enough to incorporate the large mixture of particle sizes that comprise the till. With a smaller physical measurement scale, the mini disk is predominantly influenced by the fine-grained fraction of the till. Using geometric mean K_{sat} values obtained with the double-ring and mini disk infiltrometers and available snowpack data from the 2005 water year, a physically-based hydrologic and energy-balance model was used to simulate snowpack depletion, soil moisture changes, and groundwater recharge. Simulated sediment moisture changes were used to estimate vertical flow rates toward the water table. Using a higher K_{sat} obtained at a larger physical measurement scale, the calculated flow rate 2 m below the surface is approximately three times that of the low K_{sat} scenarios. Thus, the scale dependency of hydraulic conductivity is important when quantifying groundwater recharge in mountain watersheds.

ACKNOWLEDGEMENTS

I would like to begin by expressing my gratitude for being given the opportunity to complete my Master's degree and thanking my advisor, Mike Ronayne. Without his guidance, knowledge, encouragement, and patience, I would not have been able to complete this project. I am also appreciative of my research committee: John Stednick and William Sanford. In addition to assisting me with the completion of my thesis, they inspired and supported me throughout my studies.

I am grateful for the financial support provided by the Department of Geosciences in the form of a graduate teaching assistantship and Warner Graduate Research Assistantship. I am also thankful for additional support in the form of the research grant provided by the Warner College of Natural Resources Teaching, Research, and Outreach Grants Program, through which this work was partially funded.

I would like to acknowledge and thank my field assistants: Joe Orlando, Brent Barker, Krystal Tremblay, Warren Newby, Katherine Olmo, and Stephen Saller for so willingly assisting me with field data collection.

I would also like to thank the USDA Forest Service Rocky Mountain Research Station for logistical support.

TABLE OF CONTENTS

ABSTRACT.....	ii
ACKNOWLEDGMENTS.....	iv
LIST OF FIGURES.....	vii
LIST OF TABLES.....	ix
CHAPTER 1: INTRODUCTION.....	1
1.1 Objectives.....	2
CHAPTER 2: BACKGROUND.....	4
2.1 Measuring Hydraulic Conductivity in the Field.....	4
2.1.1 Importance of Measurement Scale.....	5
2.1.2 Measurement Methods.....	5
2.1.3 Method Comparison.....	8
2.1.4 Effect of Coarse Rock Fraction.....	9
2.2 Modeling Groundwater Recharge in Mountain Environments.....	11
CHAPTER 3: STUDY SITE.....	13
3.1 Description of Study Site.....	13
3.2 Site Geology.....	14
3.3 Research Installations.....	15
3.4 Meteorological Measurements and Streamflow.....	16
3.5 GLEES Water Budget.....	16
CHAPTER 4: METHODS.....	18
4.1 Field Measurement of Hydraulic Conductivity.....	18
4.1.1 Mini Disk Infiltrometer.....	18
4.1.1.1 Experimental Procedure.....	20
4.1.1.2 Calculations.....	21
4.1.2 Double-Ring Infiltrometer.....	22
4.1.2.1 Experimental Procedure.....	22
4.1.2.2 Calculations.....	23
4.1.3 Guelph permeameter.....	23
4.1.3.1 Experimental Procedure.....	24
4.1.3.2 Calculations.....	25
4.2 Statistical Analysis of the Measured Hydraulic Conductivities.....	26

4.3 Grain Size Analysis.....	27
4.4 Estimation of Groundwater Recharge.....	27
4.4.1 Model Inputs and Initialization.....	28
4.4.2 Model Analysis.....	31
CHAPTER 5: RESULTS AND DISCUSSION.....	33
5.1 Estimated Field-Saturated Hydraulic Conductivity.....	33
5.2 Sieve Analysis.....	35
5.3 Method Comparison.....	37
5.4 Estimation of Groundwater Recharge.....	42
5.4.1 Snow Depth.....	42
5.4.2 Ground Temperature and Soil Water Content.....	43
CHAPTER 6: CONCLUSIONS.....	52
CHAPTER 7: RECOMMENDATIONS FOR FUTURE WORK.....	54
CHAPTER 8: LITERATURE CITED.....	55
APPENDIX A.....	60
APPENDIX B.....	69

LIST OF FIGURES

FIGURE 2.1: The relationship between measurement scale and saturated hydraulic conductivity.	6
FIGURE 2.2: A cross sectional view of the double-ring infiltrometer showing wetting front movement below the rings.	7
FIGURE 2.3: An illustration of the saturated zone and wetting front produced by the Guelph permeameter.	7
FIGURE 3.1: Topographic map of the West and East Glacier Lake watersheds, located in the Snowy Range, Wyoming.	14
FIGURE 4.1: Base map showing the hydraulic conductivity measurement locations. ..	19
FIGURE 4.2: Illustration of the mini disk infiltrometer.	20
FIGURE 4.3: Diagram of the Guelph permeameter.	24
FIGURE 4.4: Measured daily air temperatures collected at the GLEES tower.	29
FIGURE 4.5: Measured daily wind speeds collected at the GLEES tower.	29
FIGURE 5.1: Particle size distribution for three samples of glacial till.	35
FIGURE 5.2: Box-and-whisker plot of saturated hydraulic conductivity distributions. .	37
FIGURE 5.3: Histograms of field-saturated hydraulic conductivities estimated by the: A) mini disk infiltrometer, B) double-ring infiltrometer, and C) Guelph permeameter.	39
FIGURE 5.4: Simulated daily snow depths on north and south facing slopes at GLEES.	43
FIGURE 5.5: Simulated average daily ground temperatures during model runs on a 7.5° North (A) and South (B) facing slope using double-ring soil inputs.	44
FIGURE 5.6: Sediment moisture changes using twelve depths using a surface slope of 0.1°.	46

FIGURE 5.7: Sediment moisture changes at twelve depths using a surface slope of 7.5°. 47

FIGURE 5.8: Sediment moisture changes at twelve depths using a surface slope of 15°. 48

FIGURE 5.9: Sediment moisture changes at twelve depths using a surface slope of 29.5°. 49

FIGURE 5.10: Simulated snow depth and surface soil moisture contents plotted to show the timing of the soil moisture changes in response to melting events. 50

FIGURE 5.11: Calculated daily vertical flow rate at a depth of 2 m using K_{sat} values estimated from the larger scale measurements (A) and small scale measurements (B). 51

LIST OF TABLES

TABLE 4.1: Meteorological parameters used to drive FASST	30
TABLE 4.2: Soil parameters used by FASST. Parameters not specified by the user are set to the default values or are calculated by FASST.	30
TABLE 5.1: Estimated field-saturated hydraulic conductivity at each measurement site.	34
TABLE 5.2: Particle size distribution of the till at three sites.	36
TABLE 5.3: Median particle size and sorting.	36
TABLE 5.4: Summary statistics of estimated field-saturated hydraulic conductivity (cm/min) values determined by each method.	38

CHAPTER 1

1. INTRODUCTION

Water originating as snowmelt in mountainous watersheds is a vital resource, accounting for 50-80% of the total annual streamflow in the western United States (Day, 2009). The processes that create these mountainous watersheds often result in complex variations in topography, climatic conditions, and sediments. This complexity presents a challenge for modeling hydraulic processes in mountainous watersheds. Standard modeling practices tend to employ physically-based models in which saturated hydraulic conductivity is the most important parameter (Gupta et al., 2006). Alpine and subalpine watersheds that were sculpted by glaciation are dominated by heterogeneous sediments such as glacial till. Current measurements of alpine till hydraulic properties are limited, making further characterization necessary.

The study site selected for this research is the Glacial Lakes Ecosystem Experiments Site (GLEES), located in the Snowy Range of southeast Wyoming. Established to monitor long term environmental impacts of atmospheric deposition and climate change on alpine/subalpine ecosystems, GLEES is the site of numerous ongoing scientific studies. While not a federally mandated wilderness area, high impact activities (i.e. drilling and excavations) are prohibited within GLEES, making low impact methods for characterizing hydraulic properties necessary. Additionally, site access is limited requiring consideration given to equipment and method feasibility, transportability, and simplifying assumptions concerning heterogeneous soils. This study employs multiple

measurement techniques to characterize the field-saturated hydraulic conductivity of glacial till at GLEES.

Shaped by glaciation during the Pleistocene and Holocene, the geologic material found at GLEES is fractured bedrock and alpine glacial till, both capable of transmitting water. Glacial sediment is generally observed at the surface with minimally developed soils. Sediment hydraulic properties are affected by the presence of embedded rock fragments or, in the case of GLEES, particles ranging from gravel to large boulders.

When studying hydraulic processes within a watershed it is essential to understand the inputs and outputs of the mass water balance equation. Generating water balances that accurately represent groundwater movement within alpine/subalpine glacial tills is difficult, largely because measurements of hydraulic properties within these glacial sediments are limited. This work was undertaken in order to provide a greater understanding of the hydraulic properties governing groundwater flow within alpine tills.

1.1 Objectives

This study was undertaken to characterize the hydraulic properties of glacial sediment at GLEES, which will provide a basis for further work necessary to develop an accurate water balance at GLEES and similar sites. Around the West Glacier Lake and East Glacier Lake watersheds a double-ring infiltrometer, a mini disk infiltrometer, and Guelph permeameter were used to collect measurements of field-saturated hydraulic conductivity. The specific objectives of this study include:

- i) Determine the field-saturated hydraulic conductivity of glacial till at GLEES.

- ii) Conduct a method comparison examining how measurement technique and testing scale influence the estimated field-saturated hydraulic conductivity.
- iii) Examine the dependence of groundwater recharge on field-saturated hydraulic conductivity and land surface gradient using a physically-based near surface hydrologic model.
- iv) Evaluate how estimated groundwater recharge is influenced by field-saturated hydraulic conductivity values obtained with techniques measuring at different scales.

CHAPTER 2

2. BACKGROUND

2.1 Measuring Hydraulic Conductivity in the Field

Saturated hydraulic conductivity is commonly accepted as one of the most important properties controlling numerous hydrologic processes. Being more spatially variable than other sediment physical and hydraulic characteristics, extensive measurements are often required to obtain representative estimates of field-saturated hydraulic conductivity (Gupta et al., 2006). Measurement of field-saturated hydraulic conductivity can be conducted using different methods which often have different testing scales, boundary conditions, and underlying assumptions. Since there is no single ideal method for measuring the saturated hydraulic conductivity of highly heterogeneous sediment, selection of an appropriate method and equipment must be carefully made to obtain reliable results (Jenssen, 1990; Bagarello et al., 2009). The following literature review provides some necessary considerations when evaluating the hydraulic conductivity of glacial sediments, including measurement scale dependency and the influence of coarse rock fragments.

For this work the distinction must be made between saturated hydraulic conductivity and field-saturated hydraulic conductivity. Measuring saturated hydraulic conductivity requires complete saturation of the soil which is rarely achieved under field conditions, since some amount of air is usually entrapped in the sediment by infiltrating water. By preventing the complete saturation of the pore space, entrapped air increases

tortuosity and may result in estimates of hydraulic conductivity that are lower than those made under complete saturation (ASTM D 5126, 2004). In this study K_{sat} refers to the field-saturated hydraulic conductivity.

2.1.1 Importance of Measurement Scale

The wide mixture of particle sizes that are found in till create uncertainty when estimating hydraulic conductivity, potentially changing estimates by more than an order of magnitude spatially. Macropore systems and higher coarse particle contents often found in alpine tills both influence hydraulic conductivity and contribute to this spatial variation. Due to the heterogeneity of till, small scale measurement techniques may not provide reliable estimates of saturated hydraulic conductivity. Small scale measurements may not adequately incorporate macropores or coarse fraction resulting in either low estimates of hydraulic conductivity, commonly seen in fine soils or the matrix, or high estimated saturated hydraulic conductivity if there is an overabundance of macropores (Jenssen, 1990). For soils containing continuous macropores or large peds, Bouma (1983) suggests a sample volume of 10^5 cm^3 . When examining tills Jenssen (1990) suggested using a sample volume of 10^4 - 10^5 cm^3 . Figure 2.1 illustrates how the measurement scale may influence the estimated hydraulic conductivity value.

2.1.2 Measurement Methods

Many *in situ* methods have been developed to measure field-saturated hydraulic conductivity. However, the heterogeneity of glacial till makes some of these methods unreliable. Methods of measuring field-saturated hydraulic conductivity typically use an

infiltrometer or borehole permeameter to measure the infiltration rate of water into the surficial material. Infiltrometers generally measure conductivity at the surface and permeameters are used to measure conductivity at different depths in the subsurface profile (ASTM D 5126, 2004).

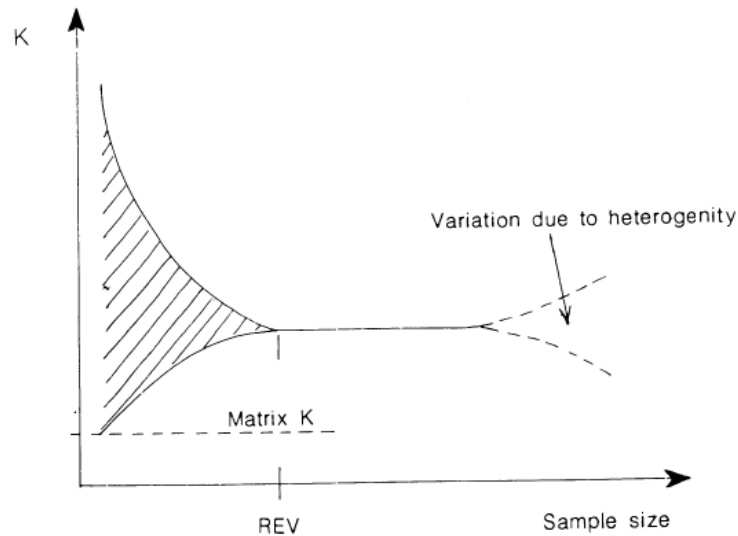


Figure 2.1: The relationship between measurement scale and saturated hydraulic conductivity proposed by Jenssen (1990). The representative elementary volume (REV) is the sample size necessary to obtain representative measurements of hydraulic conductivity.

Primary assumptions made by infiltrometers are that the volume of soil tested is field-saturated and that the K_{sat} can be determined from the measured flow rate and applied hydraulic gradient. Several other common assumptions include one-dimensional vertical flow, the wetting front is distinct and easily determined (Figure 2.2), and the presence of soil gas does not influence the movement of the wetting front (ASTM D 5126, 2004). By taking measurements at various depths in the soil profile permeameters are assumed to measure saturated hydraulic conductivity three-dimensionally (Figure 2.3).

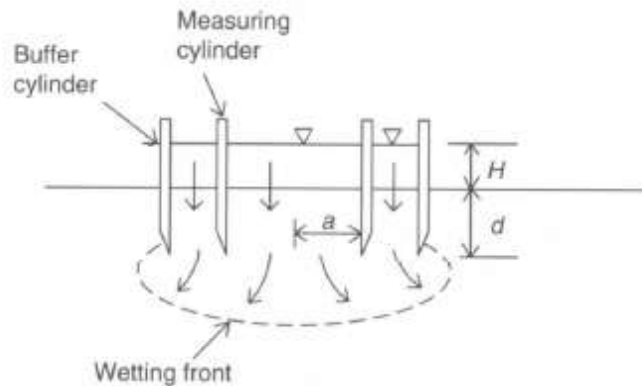


Figure 2.2: A cross sectional view of the double-ring infiltrometer showing wetting front movement below the rings. H is the depth of the ponded water or the head, d is the depth of ring insertion, and a is the inner ring radius. (Source: Reynolds, 2008b)

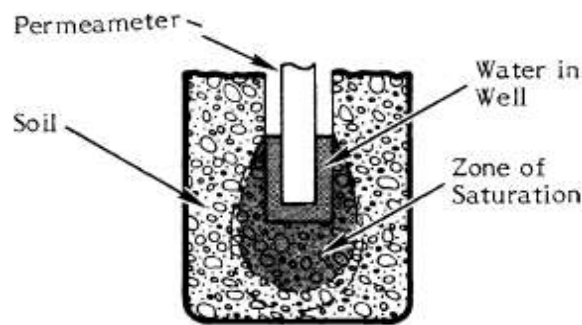


Figure 2.3: An illustration of the saturated zone and wetting front produced by the Guelph permeameter. (Source: Soil Moisture Equipment Corp., 2008)

Presently several commonly used techniques for the *in situ* measurement of field-saturated hydraulic conductivity include single-ring and double-ring infiltrometers, disk infiltrometers, air-entry permeameters, and borehole permeameters (ASTM D 5126, 2004; Cheng et al., 2011). These methods tend to rely on achieving a steady-state flow rate of water into the soil to measure field-saturated hydraulic conductivity. For this project field-saturated hydraulic conductivity was determined using the double-ring infiltrometer, the mini disk infiltrometer, and the Guelph permeameter.

2.1.3 Method Comparison

Numerous investigators have evaluated and compared different methods of measuring field-saturated hydraulic conductivity. Lee et al. (1985) compared the air-entry permeameter, Guelph permeameter, and falling-head permeameter in a variety of soil types. Significant differences seen between methods were attributed to each method's response to macropores and air entrapment. The Guelph permeameter was also found to have the lowest failure rate and, in some soils, the lowest coefficient of variation by as much as a factor of 2. In a study conducted by Kanwar et al. (1989), the Guelph permeameter was compared with a velocity permeameter. Conducted on a silt loam soil, this study found that the Guelph permeameter obtained saturated hydraulic conductivity values with greater variability than the velocity permeameters. Mohanty et al. (1994) compared saturated hydraulic conductivity measured with a Guelph permeameter, velocity permeameter, disk permeameter, and the double-tube method in a continental glacial till. The Guelph permeameter gave the lowest estimates while the disk permeameter and double-tube methods gave mean values with minimal variability. It was suggested that the low estimates were the result of measuring saturated hydraulic conductivity at a small physical scale. Both of these studies attributed the Guelph permeameter's variability to wall smearing during borehole preparation, macropore variability, or air entrapment during the initial filling (Kanwar et al., 1989; Mohanty et al., 1994; Bagarello and Provenzano, 1996). In a stony loam soil, Vanderlinden et al. (1998) compared similar methods and observed opposite results, reporting that the field-

saturated hydraulic conductivity obtained with the constant-head well permeameter and twin rings were significantly higher than the disk permeameter.

Gupta et al. (1993) compared the double-ring infiltrometer, rainfall simulator, Guelph permeameter, and Guelph infiltrometer, finding estimates provided by the double-ring infiltrometer and the Guelph permeameter were statistically the same but were significantly lower than those determined with the rainfall simulator and Guelph infiltrometer. It was also found that to obtain representative average values, the Guelph permeameter and Guelph infiltrometer require more measurements than the double-ring infiltrometer and rainfall simulator. When compared with the instantaneous profile method the Guelph permeameter measured field-saturated hydraulic conductivity values one to three orders of magnitude lower (Paige and Hillel, 1993). Paige and Hillel concluded that the instantaneous profile method was the most effective means for determining *in situ* hydraulic properties. While the above investigators propose several reasons for experiment variability they tend to neglect the natural heterogeneity of the sediment or soil.

2.1.4 Effect of Coarse Rock Fraction

Previous work indicates that measurements of saturated hydraulic conductivity are strongly affected by the presence of rock fragments and that surface and subsurface soil properties are affected differently. Defined as particles with a diameter >2 mm (Poesen and Lavee, 1994), rock fragments have been seen to restrict water movement by decreasing porosity and increasing tortuosity (Mehuys et al., 1975) whereas Sauer and

Logsdon (2002) saw the contrary with rock fragments increasing saturated hydraulic conductivity.

Poesen and Lavee (1994) examined how rock fragments affect various aspects in top soils, including the effects of rock fragments on several key hydrological processes. By separating rock fragments at the soil surface from fragments below the surface, Poesen and Lavee (1994) examined how surficial fragments affect rain fall interception, infiltration, overland flow, and evaporation and how subsurface fragments affect percolation rates which in turn affect the infiltration rate. Investigations have shown that in materials containing greater than 50% coarse rock fraction, hydraulic conductivity is not greatly affected (Peck and Watson, 1979; Bouwer and Rice, 1984; Brakensiek et al., 1986). It has also been seen that fragments within the soil reduce infiltration while surficial fragments, depending on the size, may increase or decrease infiltration (smaller rocks decrease and larger rocks increase infiltration) (Brakensiek and Rawls, 1994; Ma and Shao, 2008). Ma and Shao (2008) concluded that by making the pore structure of the fine earth fraction more favorable to water infiltration, rock fragments may increase infiltration and that the shape influences infiltration, with spherical fragments increasing infiltration compared to solid, cylindrical and rectangular, slab-like stones.

Sauer and Logsdon (2002) and Verbist et al. (2009) concluded that rock fragments will positively affect hydraulic conductivity except when the most negative pressure potentials are applied. The reason for this as suggested by Sauer and Logsdon is how the fragment adheres with the surrounding fine fraction, which will be different based on the source of the fragments (weathering in place vs. transported). Verbist et al. (2009) attributed the increase in K to a positive relation between coarse fraction and pore

space. Ravina and Magier (1984) proposed that while rock fragments increase tortuosity they also create new voids, increasing infiltration rates. Fies et al. (2002) confirmed that by preventing compaction and incomplete filling by the fine earth fraction of voids rock fragments can lead to increased porosity.

2.2 Modeling Groundwater Recharge in Mountain Environments

Models play an instrumental role in understanding processes within watersheds and developing water budgets. An area of particular interest is modeling the groundwater recharge component from a melting snowpack and how hydraulic conductivity variations may influence estimates of recharge. Snowmelt models employ two basic approaches to determine the amount of snowmelt available from a snowpack. These are an energy budget method and a temperature index method (Day, 2009). The energy budget method attempts to incorporate all factors influencing snowmelt in an energy budget equation to make the model as physically-based as possible. In comparison, the temperature index method uses basic meteorological data (mean, or maximum and minimum air temperatures) to determine snowmelt rates (Day, 2009). In an examination of a physically-based model, DeBeer and Pomeroy (2009 and 2010) used Snobal and Cold Regions Hydrological Model to estimate snowmelt and snowcover depletion in a small alpine cirque. Their findings showed that spatial variability of pre-melt Snow Water Equivalent (SWE) and spring melt rates had a significant impact on simulated snowcover depletion. They recommend considering the effects of spatial variation on SWE distribution and melt rates between slopes when modeling snowmelt dynamics and snowcover distribution in alpine environments.

The physically-based modeling program, Fast All-season Soil STrength (FASST) is a relatively new one-dimensional model, developed by the US Army Corps of Engineers (Frankenstein and Koenig, 2004). Several recent investigations have evaluated the accuracy of FASST. Holcombe (2004) compared snow cover depletion predicted by the models FASST and SNTHERM (Jordan, 1991) against observed parameters at several sites within the Rocky Mountains. It was found that while FASST was able to successfully predict the timing of snow depth changes without continuous snow depth inputs, errors arose when predicting the magnitude of snowdepth changes. Additionally, FASST was able to correctly predict the magnitude of seasonal soil moisture storage but had difficulty predicting soil moisture recharge. At two forested, sub-alpine sites, Sawyer (2007) also saw that FASST was able to accurately predict snowpack depletion. Utilizing data collected by Holcombe and Sawyer, Frankenstein et al. (2008) went on to compare FASST with SNTHERM. FASST was able to successfully reproduced snow depth predictions and was often more accurate during the snowpack development phase. The general conclusion from these studies are that while not designed to solely act as a snowpack simulation model, FASST performs well enough to be used as one, requiring less initial snowpack information than SNTHERM.

CHAPTER 3

3. STUDY SITE

3.1 Description of Study Site

Research for this project was conducted within the West and East Glacier Lakes watersheds at the Glacier Lakes Ecosystem Experiments Site (GLEES). Having the characteristics of high-elevation alpine/subalpine wilderness areas, GLEES was established to study long term environmental impacts of atmospheric chemical deposition and climate change on alpine/subalpine ecosystems (Musselman, 1994).

Encompassing approximately 575 ha with elevations ranging from 3200-3500 m, GLEES is located in the Snowy Range of Wyoming (Figure 3.1). The site latitude and longitude are 41°22'30" and 106°15'30", respectively. Located within glacial cirque basins of the prominent northeast-southwest trending ridge, the upper portion of GLEES contains three small lakes: Lost Lake, West Glacier Lake (WGL), and East Glacier Lake (EGL). The highest elevation at GLEES is 3494 m at the top of the NE-SW ridge. WGL and EGL, having respective lake stages of approximately 3276 m and 3282 m, are separated by a low wind-swept north-south trending ridge. Four drainages flow into the northern end of WGL: Boulder Creek, Meadow Creek, Cascade Creek, and Long Creek. There are no perennial streams flowing to EGL. A permanent snowfield at the top of the WGL watershed cirque supplies water to WGL (Musselman, 1994).

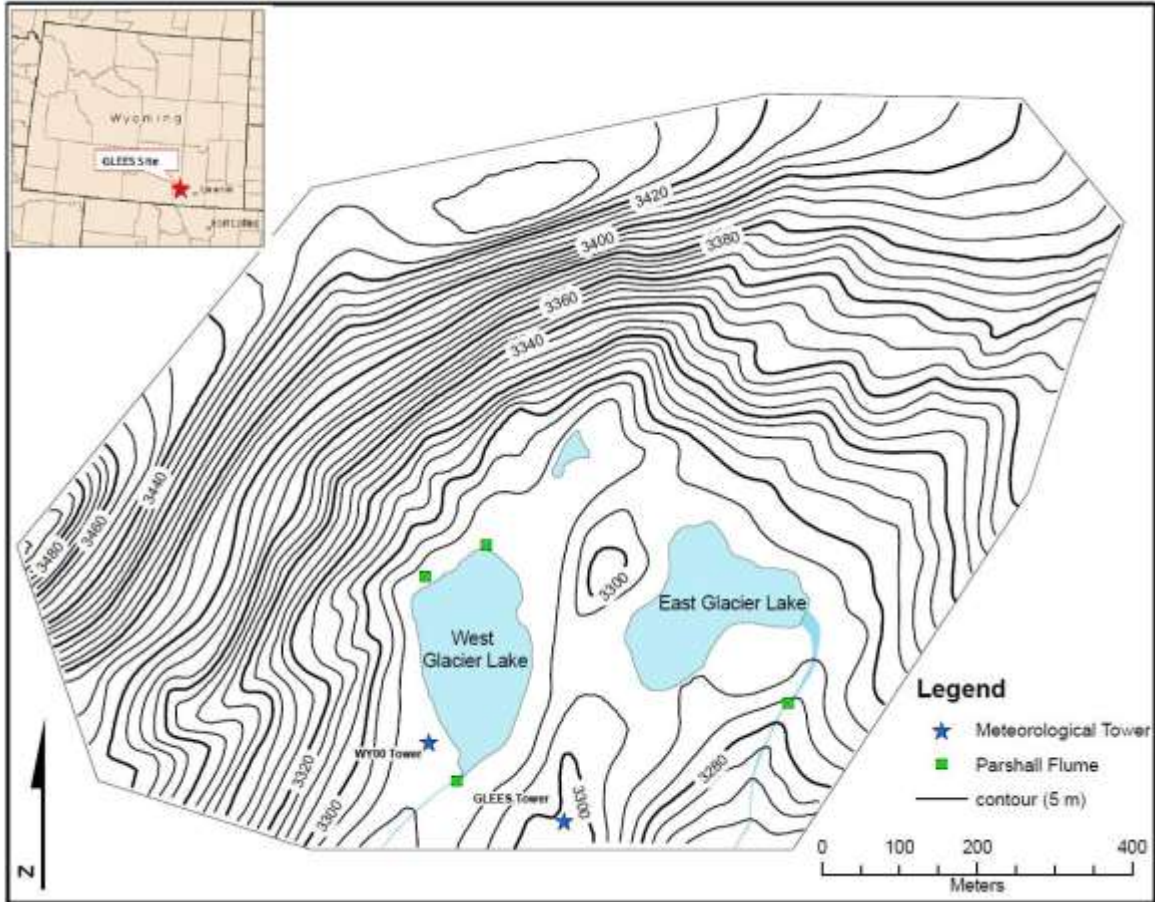


Figure 3.1: Topographic map of the West and East Glacier Lake watersheds, located in the Snowy Range, Wyoming.

3.2 Site Geology

Uplifted during the Paleocene, the Medicine Bow Mountains have a core of Precambrian rocks and contain a major shear zone known as the Cheyenne Belt. The Cheyenne Belt separates the Wyoming Province, which consists of locally intruded Archean rocks, to the northwest and accreted Proterozoic continental crust to the southeast (Rochette, 1994).

The bedrock within the study area is primarily fractured Medicine Peak Quartzite that has been intruded by mafic dikes. Alpine glaciation during the Quaternary had a significant effect on the present day geomorphology of the Snowy Range. Glaciation

carved the cirques that are now the locations of WGL and EGL and deposited till derived from local bedrock (Rochette, 1994). The glacial sediment is generally observed at the surface with minimally developed soils. Thickness of the glacial sediment is still uncertain; the most recent estimate made by Page (2011) is based on the use of ground penetrating radar to estimate a till thickness ranging from 0 to >9 m. Following glaciation the region has continued to develop through nivation, colluvial and alluvial processes and in some areas eolian processes (Hopper and Walthall, 1994).

Soil development began following glaciation, and it is believed that present day soils are at equilibrium with the climate (Rochette, 1994). Soil development varies throughout the site with minimally developed soils occurring in higher elevation areas with steep rock walls and talus slopes. Lower elevations tend to display more developed soils although the soil thickness is minimal in most areas. According to the survey conducted by Hopper (1994), the predominant soil groups found in the study site are Typic Cryoboralfs-Dystric Cryochrepts complex, Typic Cryoboralfs complex, Histic-Aeric Cryaquepts complex, and Dystric Cryochrepts-Rubbleland, quartzite complex.

3.3 Research Installations

Several research facilities have been installed at GLEES (Figure 3.1). Located to the southeast of WGL and installed in 1987, the 10 m GLEES Tower collects meteorological data. A National Atmospheric Deposition Program (NADP) wet precipitation collector and Belfort rain gage (WY00) was installed in 1986 and located on the southwest shore of WGL. Parshall flumes were installed at the WGL and EGL outlets and the Meadow and Cascade Creek inlets (Musselman, 1994).

3.4 Meteorological Measurements and Streamflow

Temperature data collected at the GLEES Tower indicate temperatures ranging from -23°C to -1°C in the winter and -7°C to 21°C during the summer (Korfmacher and Hultstrand, 2006). Precipitation occurs mostly as snow, which can occur throughout the year. The annual snowpack is usually established in November and remains into July (Sommerfeld, 1994). Precipitation and temperature data shows mean annual precipitation of 1.20 m, with 60 - 80% of this amount falling as snow. GLEES is dominated by westerly winds with speeds ranging from 0 to 26 m/s with an average of 8 m/s (Hultstrand, 2006).

3.5 GLEES Water Budget

Generation of a water budget requires using a conservation of mass equation to account for water within the system over a given period of time. The general form of this equation states that the sum of inputs (I) and outputs (O) is equal to the change in storage (ΔS) over a given period of time:

$$I - O = \Delta S \qquad \text{Equation 3.1}$$

This equation can be adapted to provide a more detailed form with site-specific components. To account for the particular conditions at GLEES this equation can be written as follows:

$$\begin{aligned}
P^{rain} + P^{snow} - Q_{out}^{SW} - Q_{out}^{GW} - ET - E^{snow} \\
= \Delta S^{SW} + \Delta S^{snow} + \Delta S^{UZ} + \Delta S^{GW}
\end{aligned}
\tag{Equation 3.2}$$

where P^{rain} and P^{snow} are the precipitation inflows from snow and rain, Q_{out}^{SW} is the surface water outflow in streams, Q_{out}^{GW} is the groundwater outflow, ET is the loss due to evapotranspiration, and E^{snow} is snowpack sublimation. The ΔS components represent changes in: storage of surface water bodies (SW), snowpack ($snow$), unsaturated zone (UZ), and saturated zone (GW) (Healy et al., 2007).

The Q_{out} groundwater term represents an important unknown for the water balance at GLEES. This knowledge gap is a major motivation for the hydrogeologic field characterization presented in this study.

CHAPTER 4

4. METHODS

4.1 Field Measurement of Hydraulic Conductivity

Measurements of field-saturated hydraulic conductivity (K_{sat}) were conducted August through September 2009 and July through August 2010. At 32 locations around West and East Glacier Lakes (Figure 4.1), K_{sat} measurements were obtained using: a mini disk infiltrometer, a double-ring infiltrometer, and a Guelph permeameter. Selection of test locations was based on proximity to previous test sites, land surface gradient, and surface conditions (the primary limitation was the ability to install the double-ring infiltrometer's inner and outer rings with minimal sediment disturbance). At each location testing began by placing the inner and outer rings for the double-ring infiltrometer. Following the installation of the rings, three mini disk infiltrometer tests were conducted at undisturbed points within the annular space. Following the mini disk tests, K_{sat} was determined with the double-ring infiltrometer and then the Guelph permeameter.

4.1.1 Mini Disk Infiltrator

The mini disk infiltrometer (Figure 4.2) is a portable tension infiltrometer that determines the field-saturated hydraulic conductivity (K_{sat}) and sorptivity (S) by tracking cumulative infiltration through time (Zhang, 1997). The device has a main tube (water reservoir) with a diameter of 3.1 cm and a 4.5-cm diameter stainless steel disk which

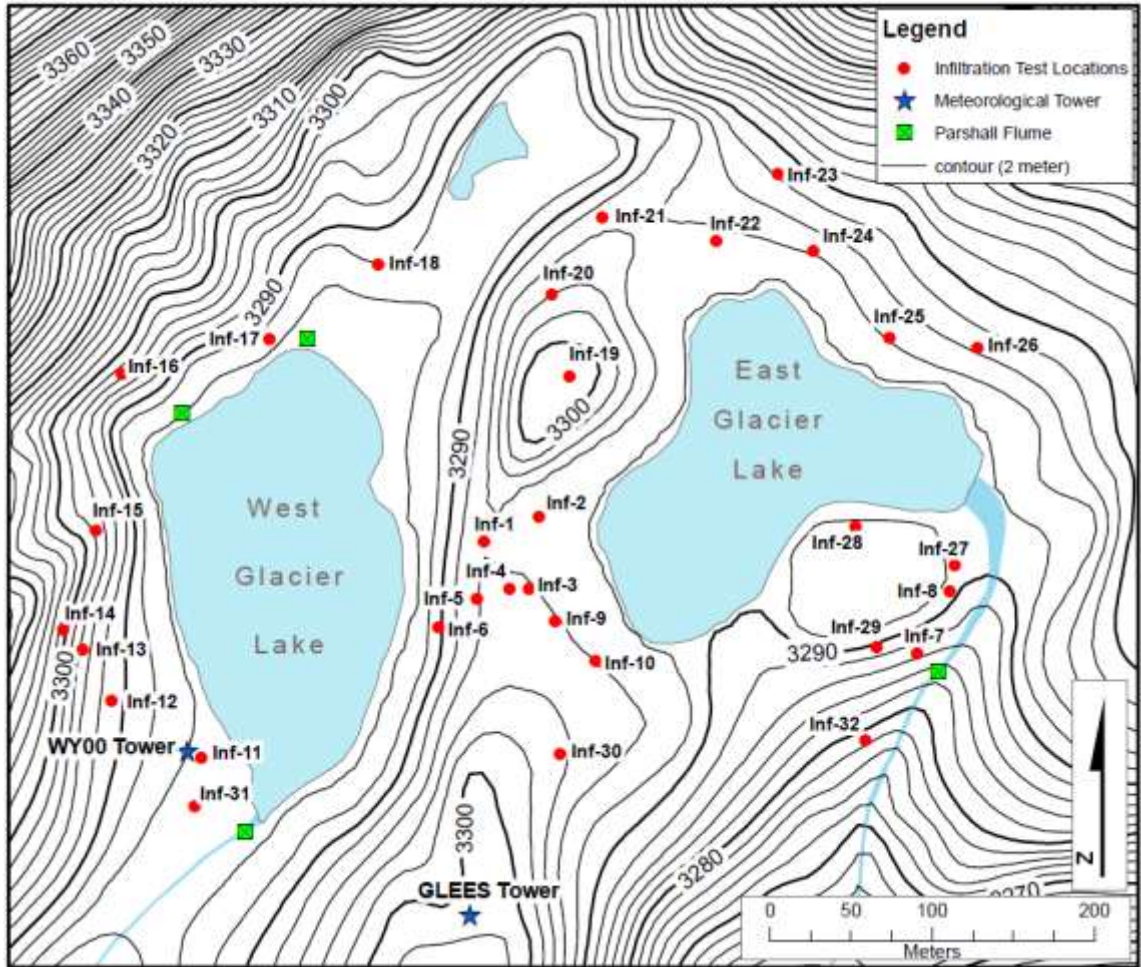


Figure 4.1: Base map showing the hydraulic conductivity measurement locations.

makes contact with the surficial material at the base of the tube. A bubble chamber at the top of the apparatus allows for tension control. Controlling the tension allows the mini disk infiltrometer to eliminate macropores by preventing filling of pores with an air entry value less than the applied tension (Decagon Devices, Inc., 2007). By controlling macropore flow and taking measurements at the sediment surface this instrument allows for undisturbed measurements of the sediment and measures the hydraulic properties of the fine earth component. Pressure head is controlled at the top of the device with the bubbling chamber and moveable air-entry tube.

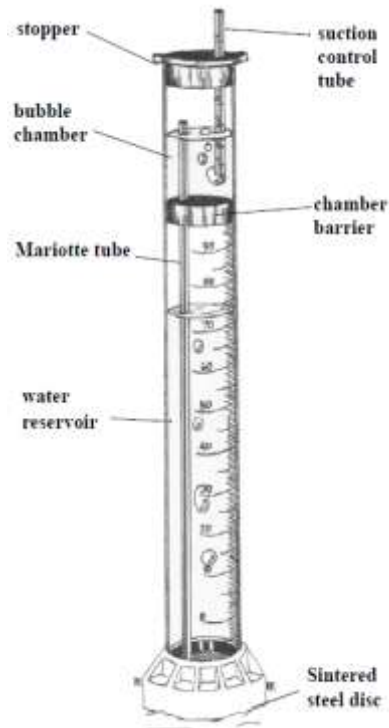


Figure 4.2: Illustration of the mini disk infiltrometer (Source: Decagon Devices, Inc., 2007)

4.1.1.1 Experimental Procedure

At each location three mini disk tests were conducted using the procedure recommended in the mini disk infiltrometer manual (Decagon Devices, Inc., 2007). Prior to beginning the tests the rings used for the double-ring infiltrometer were prepared; see section 4.1.2.1 for placement method. These tests were conducted at three undisturbed points within the infiltrometers's annular space. Since different soils infiltrate water at different rates, the applied tension varied between locations. According to the manual a tension of 2 cm is sufficient for most soils (Decagon Devices, Inc., 2007). Each test was run a minimum of 8 to 10 minutes or until at least 15-20 mL of water had infiltrated.

4.1.1.2 Calculations

Three estimates of K_{sat} were determined at each test location using the approach proposed by Zhang (1997). This method requires plotting the cumulative infiltration (I , cm) vs. the square root of time (t , min) and fitting with the following function:

$$I = C_1 t + C_2 t^{1/2} \quad \text{Equation 4.1}$$

where C_1 (cm min^{-1}) is a parameter relating to the hydraulic conductivity, and the parameter C_2 ($\text{cm min}^{-1/2}$) is related to the soil sorptivity. Using C_1 at the applied tension, K_{sat} was determined using the following relationship:

$$K_{sat} = \frac{C_1}{a} \quad \text{Equation 4.2}$$

where K_{sat} (cm/min) is the field-saturated hydraulic conductivity, a is a dimensionless coefficient dependent on disk diameter, applied tension, and van Genuchten soil parameters for the appropriate soil texture. Using the van Genuchten retention parameters for a silt loam, the coefficient a is determined using the following relationship proposed by Zhang (1997):

$$a = \frac{11.65(n^{0.1} - 1)\exp[7.5(n - 1.9)ah_0]}{(\alpha r_0)^{0.91}} \quad n < 1.9 \quad \text{Equation 4.3}$$

where n and α are the respective van Genuchten retention parameters of 1.41 and 0.020 cm^{-1} , r_o is the radius of the infiltrometer disk (2.25 cm), and h_o (cm) is the applied tension.

4.1.2 Double-Ring Infiltrometer

The double-ring infiltrometer is a well-established field method for measuring infiltration and determining K_{sat} . This method determines K_{sat} by measuring the volume of water necessary to maintain a constant head within the inner ring until steady-state flow is achieved (ASTM D 5126, 2004). The double-ring infiltrometer uses an outer ring to create an annular space between the two rings to promote one-dimensional, vertical flow from the inner ring by minimizing edge and divergence effects (Bouwer, 1986).

4.1.2.1 Experimental Procedure

The inner and outer rings having respective diameters of 30.5 cm and 61.0 cm with a height of 50.80 cm were driven into the ground with the inner ring centered within the outer ring. Following the standard procedure (ASTM D 3385, 2003), each ring was driven into the ground to a depth necessary to maintain an adequate seal, approximately 7 to 11 cm. When placing the rings care was taken to ensure minimal disturbance of the sediment surface. If the disturbance was too great the rings were removed and replaced at a new location. Following ring installation the desired water level was marked on the rings and each ring was filled. A constant head in the inner ring was maintained using a graduated Mariotte tube. During the experiment, the water level was initially recorded every 5 or 10 min and were eventually increased to 20 min intervals. Each test was run

until a steady-state flow rate was reached (i.e. when the volume of water added during each time step became nearly constant), approximately 1.5 to 2 hours (ASTM Standard D 3385, 2003). Using this information the infiltration rate was determined. If during the experiment it began to rain, the equipment was covered to avoid the addition of an unknown quantity of precipitation water.

4.1.2.2 Calculations

The steady-state infiltration rate of the inner ring was determined according to the ASTM Standard D 3385 (2003) standard procedure. Using Darcy’s law and assuming a unit hydraulic gradient, the K_{sat} is equivalent to the steady-state infiltration rate. The infiltration rate (i , cm/hr) was calculated for each time step using:

$$i = \frac{Q_{ir}}{A_{ir}} \quad \text{Equation 4.4}$$

where Q_{ir} is the total discharge from the inner ring (cm^3/hrs), and A_{ir} is the area of the inner ring (729.7 cm^2).

Infiltration curves for each test location were created using the data. Field-saturated hydraulic conductivity estimates were based on the final infiltration value or were estimated from the infiltration curve.

4.1.3 Guelph permeameter

The Guelph permeameter (Figure 4.3) is a widely used constant-head well permeameter capable of *in situ* measurements of field-saturated hydraulic conductivity

(K_{sat}) (Reynolds and Elrick, 1986). This measurement technique involves ponding one or more constant heads in an uncased borehole and measuring the flow of water out of the borehole until a steady-state flow rate is achieved (Bagarello, 1996; Reynolds, 2008a).

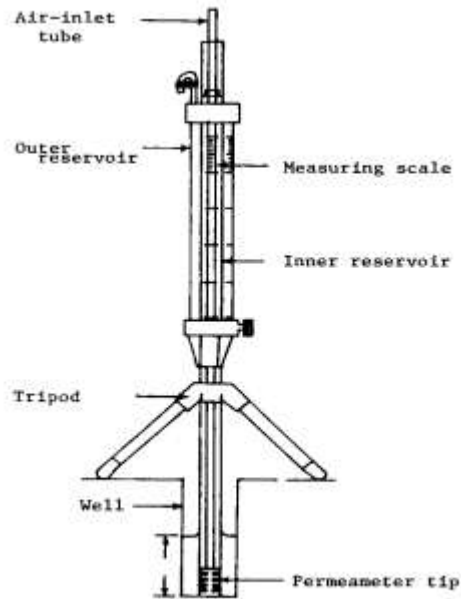


Figure 4.3: Diagram of the Guelph permeameter (Source: Kanwar et al., 1989)

4.1.3.1 Experimental Procedure

The standard procedure presented in the Model 2800K1 Guelph permeameter manual provided assembly instructions and test methods (Soil Moisture Equipment Corp., 2008). Using the soil and sizing auger a 8 to 15 cm deep borehole with a uniform diameter of 5 cm was excavated. Following borehole excavation a borehole prep brush was used to remove auger induced wall smearing (Reynolds, 2008a).

Due to the sediment heterogeneity, borehole depth varied between locations, which required using different heads for each test location. At each test location the steady-state discharge values corresponding to two heads (H_1 and H_2) were measured. Each head was based on the borehole depth; if the borehole was >11 cm deep H_1 was

5cm and H_2 was 10cm. If the borehole was <11 cm, 1cm was subtracted from the total depth which was H_2 and halved for H_1 . At each head the rate of fall (R_1 and R_2) was measured at regular time intervals of 1 or 2 minutes. The test was conducted until R at each head remained constant for 3 consecutive time intervals (a steady-state rate of fall of water in the reservoir had been achieved) (Soil Moisture Equipment Corp., 2008).

4.1.3.2 Calculations

Using the two-head analysis developed by Reynolds and Elrick (1986), the K_{sat} was calculated as follows:

$$K_{sat} = G_2 Q_2 - G_1 Q_1 \quad \text{Equation 4.5}$$

where:

$$Q_1 = X * R_1 \text{ or } Y * R_1 \quad \text{Equation 4.6a}$$

$$Q_2 = X * R_2 \text{ or } Y * R_2 \quad \text{Equation 4.6b}$$

where X is the cross sectional area of the combination reservoir (35.54 cm^2) and Y is the cross sectional area of the inner reservoir (2.15 cm^2). R_1 and R_2 are the steady-state flow rates corresponding to each head level (H_1 and H_2).

$$G_1 = \frac{H_2 C_1}{\pi(2H_1 H_2 (H_2 - H_1) + a^2 (H_1 C_2 - H_2 C_1))} \quad \text{Equation 4.7a}$$

$$G_2 = \frac{H_1 C_2}{\pi(2H_1 H_2 (H_2 - H_1) + a^2 (H_1 C_2 - H_2 C_1))} \quad \text{Equation 4.7b}$$

where:

$$C_1 = \left(\frac{H_1/a}{2.074 + 0.093 \left(\frac{H_1}{a} \right)} \right)^{0.754} \quad \text{Equation 4.8a}$$

$$C_2 = \left(\frac{H_2/a}{1.992 + 0.091 \left(\frac{H_2}{a} \right)} \right)^{0.683} \quad \text{Equation 4.8b}$$

C_1 and C_2 are shape factors corresponding to the H_1/a and H_2/a ratios, and a is the borehole radius (cm) (Soilmoisture Equipment Corp., 2008).

4.2 Statistical Analysis of the Measured Hydraulic Conductivities

Estimated K_{sat} values were statistically compared on the basis of arithmetic and geometric means, standard deviation (SD), coefficient of variation (CV), range, lower (Q1) and upper (Q3) quartiles, and failure rate (FR). As a better indicator of the population's central tendency, the geometric mean was used to compare average values for each method. A failure is defined as an unsuccessful measurement attempt that did not allow for an estimation of K_{sat} . The Statistical Analysis Software (SAS) package was used employed for the analysis (SAS Institute Inc., 2010).

4.3 Grain Size Analysis

Grain size analysis was conducted on samples of till collected at sites 5, 6, and 14 (Figure 4.1). Although the till at GLEES contains a broad distribution of particle sizes the collected samples contained particles no larger than cobbles. There are various classification schemes where particle size limits vary, but it is generally accepted that a particle diameter of 2 mm is the lower threshold of “coarse fraction” (Rawls et al., 1993). Based on the USDA classification system, the coarse fraction, sand, silt, and clay contents were determined. Using sieves the coarse fraction was subdivided into six categories: cobbles (particle diameters $>76.2\text{mm}$), coarse gravel (particle diameters of $>50.8\text{mm}$, $>25.4\text{mm}$ and $>12.7\text{mm}$), and fine gravel (particle diameters $>6.35\text{mm}$ and $>2\text{mm}$). Sand was separated into three fractions containing very coarse sand (particle diameters $>1\text{mm}$), coarse to medium sand (particle diameters $>0.25\text{mm}$), and fine to very fine sand (particle diameters $>0.05\text{mm}$). Silt and clay sized particles ($>0.002\text{mm}$ and $<0.002\text{mm}$ diameter, respectively) were separated using the hydrometer method (ASTM D 422, 2007; Gee and Bauder, 1986).

4.4 Estimation of Groundwater Recharge

To gain a more complete understanding of the groundwater component at GLEES and learn where additional data are needed, FASST was used to provide preliminary model calculations on the snowmelt contribution to groundwater recharge. The fundamental operations of FASST allow for the calculation of an energy and water budget that considers both the flow of heat and moisture within the soil, and also the

exchange of heat and moisture at all interfaces (ground/air or ground/snow; snow/air). The FASST code is documented in Frankenstein and Koenig (2004).

4.4.1 Model Inputs and Initialization

Examination of how K_{sat} and slope influence snowmelt infiltration required creating models using combinations of averaged mini disk infiltrometer and double-ring infiltrometer's K_{sat} estimates, representative land surface gradient, and aspect angles of 0.0° and 180° . Using data from the 2005 water year, FASST was initialized on April 20, 2005, which is the approximate date of maximum snow accumulation identified by Hultstrand (2006). Each model simulation was run through September 30, 2005. Within the WGL watershed Hultstrand (2006) calculated the mean peak accumulation snowpack depth of 1.82 m and snow water equivalent (SWE) of 1.06 m. Models did not account for additional precipitation occurring after peak accumulation.

The model initialization assumed no ice layer between the soil surface and snowpack. A surface roughness length of 0.01 m (Brock et. al., 2006) was specified. Driving meteorological data consisted of hourly air temperatures (Figure 4.4) and measured wind speeds and directions obtained from GLEES tower (Figure 4.5) (Korfmacher and Hultstrand, 2006). Unknown meteorological parameters were set to the default values within FASST or set using representative values for an elevation of 3300 m. Initial surface albedo was set to 0.35. A list of the meteorological values used in the simulations is provided in Table 4.1.

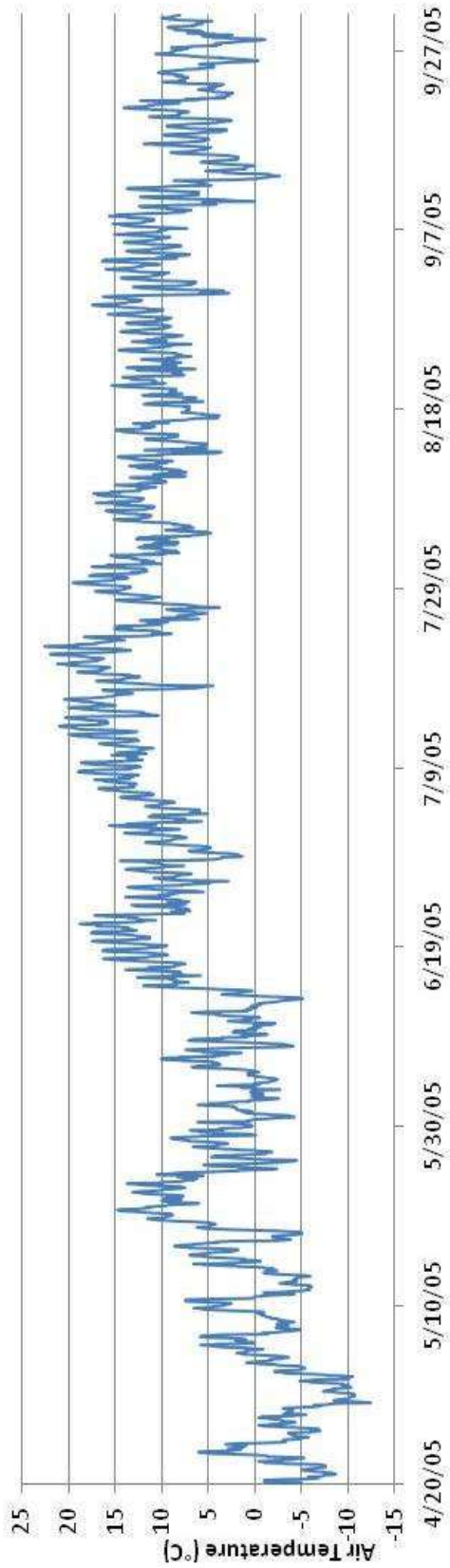


Figure 4.4: Measured daily air temperatures collected at the GLEES tower.

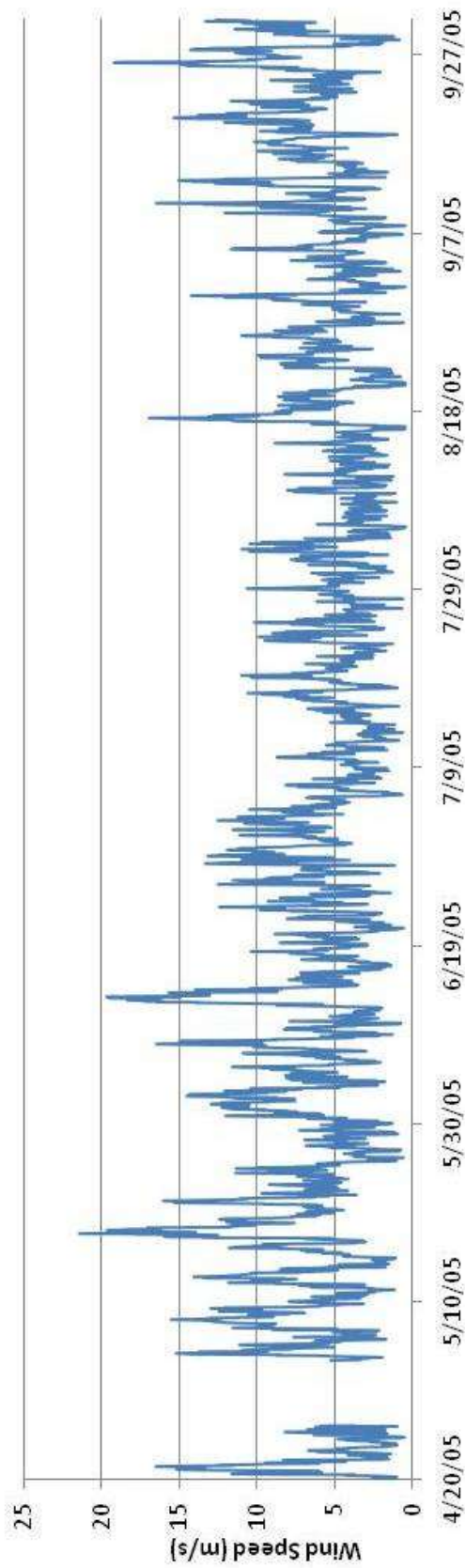


Figure 4.5: Measured daily wind speeds collected at the GLEES tower.

Table 4.1: Meteorological parameters used to drive FASST (Frankenstein and Koenig, 2004).

Parameter	Value
Air Pressure	700 mbar
Relative Humidity	60%
Precipitation Rate	0.0 mm/hr
Precipitation Type	1 (none)
Low Cloud Amount	0.5 tenths
Low Cloud Height	Model will calculate based on season and latitude
Low Cloud Type	6 (stratus nebulosus or stratus fractus)
Middle Cloud Amount	0.0 tenths
Middle Cloud Height	Model will calculate based on season and latitude
Middle Cloud Type	3 altocumulus translucidus, 1 level
High Cloud Amount	0.0 tenths
High Cloud Height	Model will calculate based on season and latitude
High Cloud Type	5 (cirrus and/or cirrostratus < 45° above the horizon) if High Cloud Amount < 0.4 7 (cirrostratus, full cover) if High Cloud Amount > 0.4

Table 4.2: Sediment parameters used in the model simulations (Frankenstein and Koenig, 2004).

Parameter	Value
Bulk density of dry material	1.640 g/cm ³
Porosity	0.385
Albedo	0.35
Emissivity	0.92
Specific heat of dry material	850.60 J/kg*K
Residual water content	0.010 vol/vol
Maximum water content	0.385 vol/vol
van Genuchten constant (α)	0.0187 cm ⁻¹
van Genuchten exponent (n)	2.16

Soil properties used for the FASST simulations are listed in Table 4.2. Where site-specific measurements were not available for a given property, representative literature values for silty sands, sand-silt mixtures (USCS soil type “SM”) were used (Frankenstein and Koenig, 2004). To evaluate the sensitivity to the hydraulic conductivity, two K_{sat} values were considered in the simulations: the geometric mean

obtained with the mini disk infiltrometer (2.8×10^{-4} cm/sec) and double-ring infiltrometer (2.7×10^{-3} cm/sec).

Four slopes were considered; in the vicinity of the test sites three representative slopes (0.1° , 7.5° , and 15°) were determined from a topographic map, and the WGL watershed mean slope of 29.5° presented by Hultstrand (2006).

4.4.2 Model Analysis

Simulated snowpack depletion and ground information were used to evaluate how the average K_{sat} values obtained with different measurement techniques influence estimates of recharge from snowmelt. The one-dimensional simulation domain was discretized using 12 nodes at depths ranging from 0 to 2 m. A finer discretization was used near the land surface to deal with steep moisture gradients immediately beneath the surface. Using the simulated moisture content at depths of 1.785 m and 2 m for each scenario, the total volume of water available for recharge during the duration of the run and the flow rate at a depth of 2 m were calculated. The flow rate was calculated using Darcy's law with the unsaturated hydraulic conductivity obtained using the van Genuchten (1980) soil water retention and hydraulic conductivity relationships.

$$Q_{vertical} = K(\theta) * A * \frac{\Delta H}{\Delta Z} \quad \text{Equation 4.10}$$

where $Q_{vertical}$ is the flow rate (cm^3/sec) through a cross sectional area A (cm^2), $K(\theta)$ is the hydraulic conductivity (cm/sec) for a given water content (θ), ΔH (cm) is the difference in hydraulic heads, and ΔZ (cm) in the change in depth. The hydraulic

conductivity as a function of volumetric moisture content ($K(\theta)$) was calculated for each time step using (van Genuchten 1980):

$$K(\theta) = K_{sat} \left(\frac{\theta - \theta_r}{\phi - \theta_r} \right)^{1/2} \left\{ 1 - \left[1 - \left(\frac{\theta - \theta_r}{\phi - \theta_r} \right)^{n/(n-1)} \right]^{1-1/n} \right\}^2 \quad \text{Equation 4.11}$$

where K_{sat} (cm/sec) is the saturated hydraulic conductivity, θ is the water content at the given time step, θ_r is the residual water content equal to 0.01, ϕ is the porosity equal to 0.385, and n and α are van Genuchten curve shape parameters with respective values of 2.16 and 0.0187 cm^{-1} (Table 1). The moisture content simulated by FASST was converted to a pressure head (ψ) using van Genuchten's (1980) moisture retention model. The total hydraulic head at each depth was determined by taking the sum of the pressure head (ψ) and elevation head (z):

$$H = \psi + z \quad \text{Equation 4.12}$$

using a datum at 2 m below ground surface. Thus, the elevation heads for the upper and lower depth planes are 0.215 m and 0 m, respectively. The simulated total head values were used along with the unsaturated hydraulic conductivity to determine vertical flow rates (Equation 4.10). These flow rates are reported as the recharge quantities in Section 5.4.2.

CHAPTER 5

5. RESULTS AND DISCUSSION

5.1 Estimated Field-Saturated Hydraulic Conductivity

Measured K_{sat} values obtained from each method are summarized in Table 5.1. While all three measurement methods were attempted at each of the 32 sites, 29 of the double-ring infiltrometer estimates and 27 of the Guelph permeameter estimates were used for analysis. In the case of the double-ring infiltrometer, a site was removed if a steady infiltration rate could not be identified. Guelph permeameter estimates were omitted when K_{sat} values were negative or the reservoir ran out of water before achieving steady flow rate. At least two methods were successfully conducted at each site except Site 6. Placement of the rings at Site 6 was problematic with several initial unsuccessful attempts placing the rings. This site is on the slope leading down to WGL where erosive processes have exposed more of the coarse fraction, making ring placement and borehole auguring for the Guelph permeameter problematic. Cumulative infiltration plots, along with the best-fit polynomials and coefficient values, used to determine K_{sat} for the mini disk infiltrometer are presented in Appendix A. The double-ring infiltrometer infiltration curves are presented in Appendix B.

Table 5.1: Estimated field-saturated hydraulic conductivity at each measurement site.

Site	Mini Disk Infiltrometer (cm/min)	Double-Ring Infiltrometer (cm/min)	Guelph permeameter (cm/min)
1	0.0152	0.055	0.77551
2	0.0155	0.050	0.02991
3	0.0079	0.013	0.33828
4	0.0155	-	0.21102
5	0.0119	0.051	0.07317
6	0.0319	-	-
7	0.0052	0.281	0.01894
8	0.0100	-	0.02891
9	0.0206	0.36	0.0795
10	0.0182	0.13	0.3305
11	0.0143	0.085	-
12	0.0111	0.19	0.1554
13	0.0169	0.08	0.0500
14	0.0102	0.06	0.1098
15	0.0209	0.24	0.0808
16	0.0158	0.2	0.2013
17	0.0104	0.17	0.0326
18	0.0352	0.22	0.2823
19	0.0151	0.19	0.0955
20	0.0089	0.12	-
21	0.0260	0.2	0.0848
22	0.0151	0.11	0.1724
23	0.0124	0.14	0.0515
24	0.0382	0.34	0.0470
25	0.0017	0.19	0.3789
26	0.0129	0.09	0.1439
27	0.0097	0.40	0.0730
28	0.0107	0.13	-
29	0.0115	0.06	0.0840
30	0.0137	0.10	-
31	0.0432	0.4	0.22871
32	0.0280	0.01	0.00313

5.2 Sieve Analysis

The grain size distribution curves (Figure 5.1) illustrate the extreme mixture of particle sizes within the glacial till. Table 5.2 lists the percent amounts of coarse fraction, sand, silt, and clay for each sample. The d_{10} , d_{50} , d_{60} , and uniformity coefficient (C_u) for the three sites are summarized in Table 5.3. The large C_u values further demonstrate the broad distribution of grain sizes and that the till has no representative grain size diameter. Even though only three till samples were analyzed, the samples provide insight into the till composition. Similar grain size distributions at sites 5 and 14 indicate that the makeup of the till is similar around the WGL watershed.

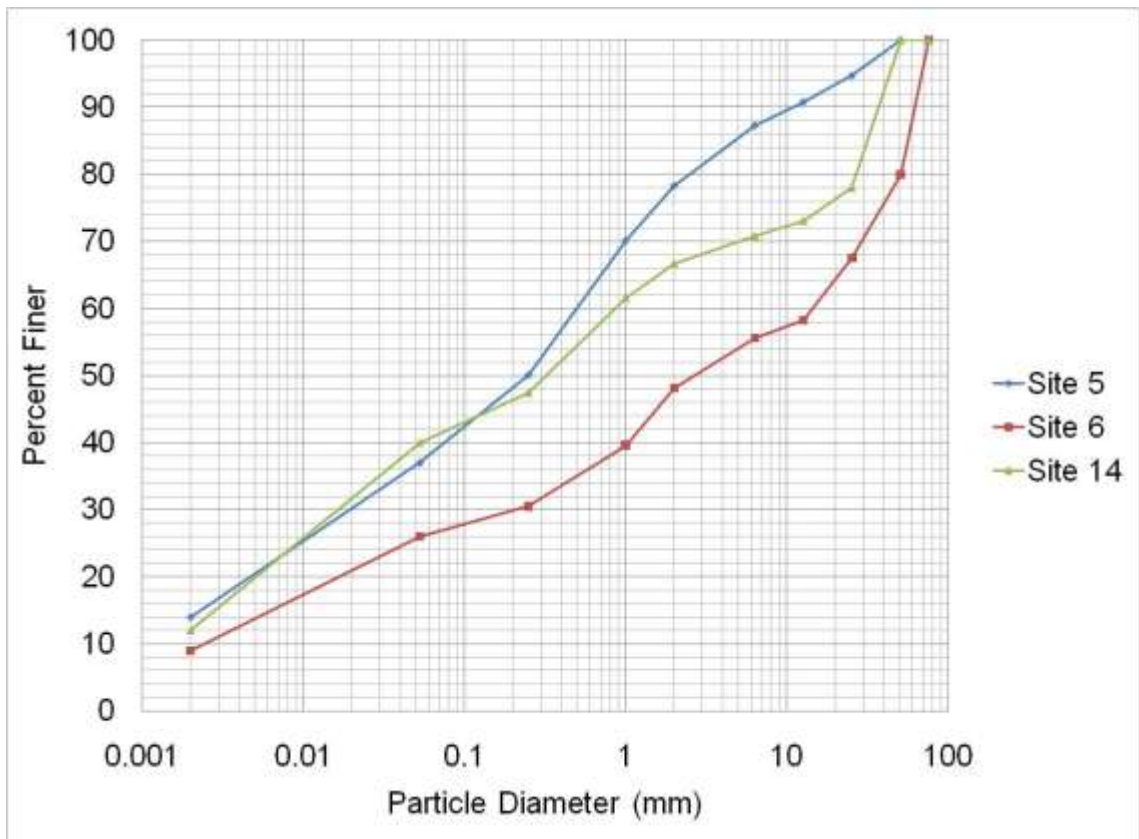


Figure 5.1: Particle size distribution for three samples of glacial till. The detailed particle size data are presented in Table 5.3

Table 5.2: Particle size distribution of the till at three sites.

Site #	% retained by the following sieve sizes (mm)										Hydrometer		
	76.2	50.8	25.4	12.7	6.35	2.0	1.0	0.25	0.053	0.002	0.0002	silt	clay
5	0	0	5.3	3.9	3.5	9.0	8.2	20.0	13.1	23	14		
6	0	20	12.5	9.3	2.6	7.5	8.5	9.1	4.5	17	9		
14	0	0	22.0	4.9	2.3	4.1	5.1	14.1	7.5	28	12		

Table 5.3: Median particle size and sorting.

Site #	d ₅₀	d ₁₀	d ₆₀	C _u
5	.25	.001	.5	500
6	2.7	.0026	15	5769.23
14	.32	.0014	.87	621.43

5.3 Method Comparison

The means and ranges of the K_{sat} values obtained by each method are displayed as side-by-side box-and-whisker plots in Figure 5.2 with corresponding descriptive statistics in Table 5.4. As is common for measured hydraulic properties, the data are best described with a log normal distribution (Figures 5.3a-c) (Warrick and Nielsen, 1980).

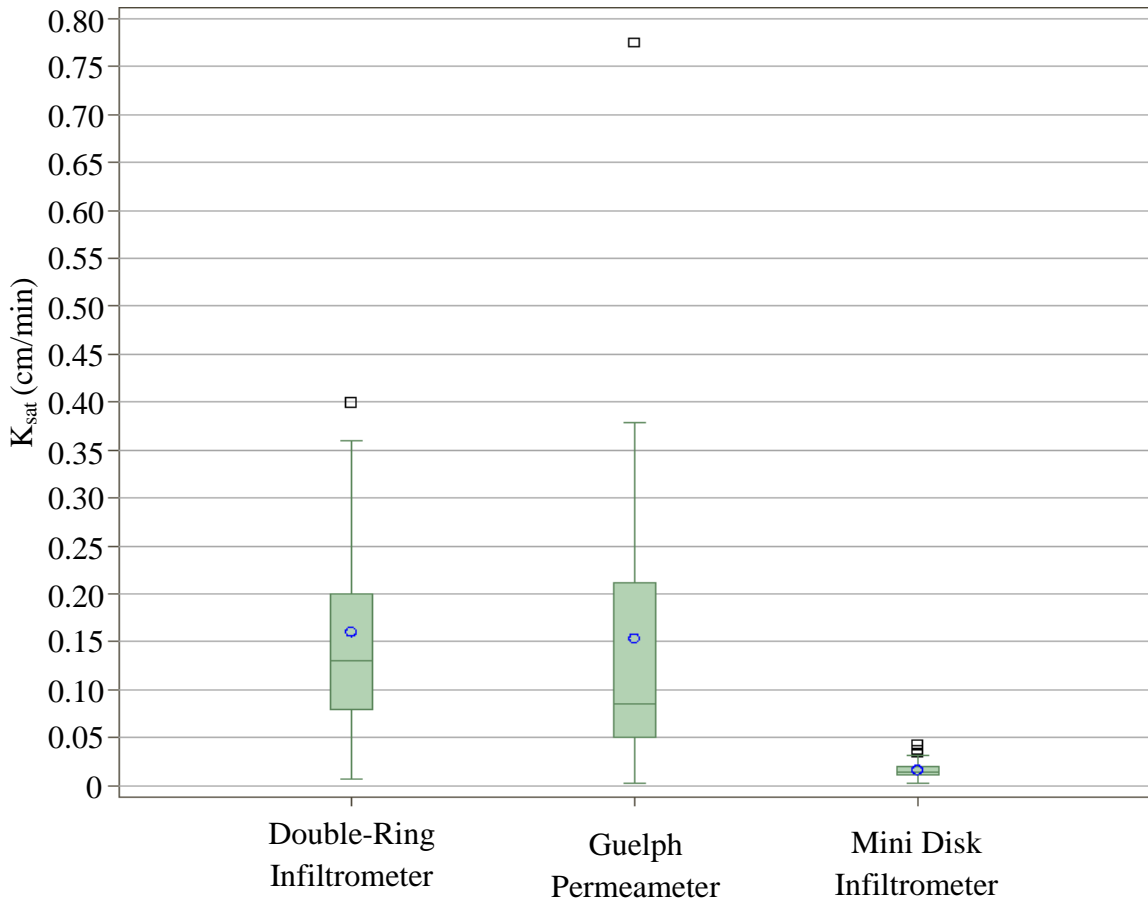


Figure 5.2: Box-and-whisker plots of field-saturated hydraulic conductivity distributions. The arithmetic mean is shown as the open circle. Whiskers were fitted with fences to separate K_{sat} values 1.5 times beyond the interquartile range (IQR); the lower fence equals $Q1-1.5*(IQR)$ and the upper fence is $Q3+1.5*(IQR)$.

Table 5.4: Summary statistics of estimated field-saturated hydraulic conductivity (cm/min) values determined by each method.

Method	Number of Tests	Min	Q1	Arithmetic Mean	Geometric Mean	Q3	Max	SD	CV	Range
Mini Disk Infiltrometer	32	0.002	0.0105	0.0167	0.0142	0.0195	0.043	0.0095	57.022	0.041
Double-Ring Infiltrometer	29	0.007	0.080	0.161	0.118	0.200	0.400	0.111	69.056	0.393
Guelph Permeameter	27	0.003	0.050	0.154	0.0939	0.211	0.776	0.163	105.598	0.773

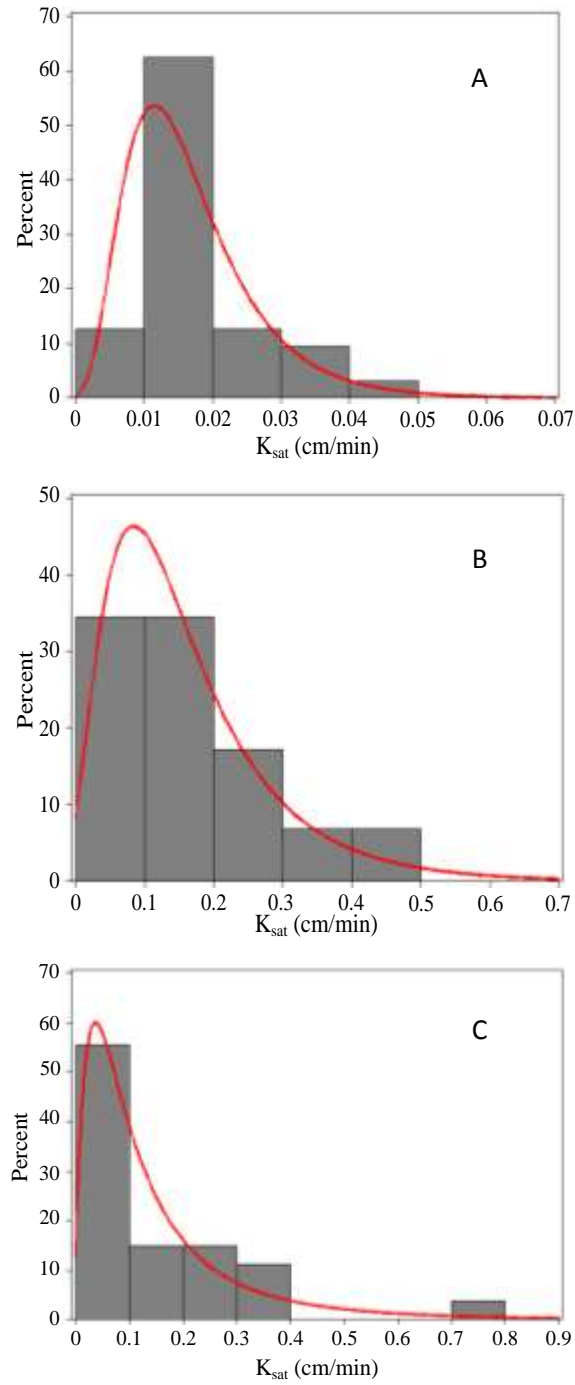


Figure 5.3: Histograms of field-saturated hydraulic conductivities estimated by the: A) mini disk infiltrometer, B) double-ring infiltrometer, and C) Guelph permeameter. The solid line shows the population theoretical distribution, based on the 32 sample locations.

Geometric mean K_{sat} values obtained with the double-ring infiltrometer and Guelph permeameter were 0.12 cm/min and 0.094 cm/min, respectively. The mini disk infiltrometer had a geometric mean K_{sat} that was nearly an order of magnitude lower, at 0.014 cm/min. Comparison of the means suggests there is not a significant difference between the double-ring infiltrometer and the Guelph permeameter, but the difference between these two and the mini disk infiltrometer is significant. The similarities between the double-ring infiltrometer and Guelph permeameter show that the two methods are measuring the K_{sat} at similar scales while the mini disk infiltrometer is testing at a much smaller scale.

The double-ring infiltrometer and the Guelph permeameter had similar ranges with the double-ring infiltrometer ranging from 0.007 cm/min to 0.40 cm/min and the Guelph ranging from 0.003 cm/min to 0.776 cm/min. The mini disk infiltrometer ranged from 0.002 cm/min to 0.043 cm/min. Examination of the inner quartile range (IQR) and fences shows that while the Guelph permeameter has a range nearly twice that of the double-ring infiltrometer, the Guelph permeameter having one large value at 0.776 cm/min. Several possibilities for this extreme value include experimental error, excessive disturbance of the soil when preparing the borehole, presence of a nearby macropore, and/or a zone within the till that has a higher hydraulic conductivity (Kanwar et al., 1989; Mohanty et al., 1994).

Table 5.4 shows that there is an increase in the standard deviation (SD) and coefficient of variation (CV) obtained by the Guelph permeameter. Having an SD of 0.163 and CV of 105.60%, the Guelph permeameter has the greatest variability in K_{sat} compared to the other methods. This high CV is partly caused by the single high

estimate of K_{sat} at 0.776 cm/min. While the double-ring infiltrometer obtained a similar SD at 0.111, its CV is closer to that of the mini disk infiltrometer. The mini disk infiltrometer had the lowest SD at 0.0095. The mini disk and double-ring infiltrometers yielded K_{sat} values with CV of 57.02% and 69.06%, respectively. Gupta et al. (1993) also found that K_{sat} values obtained using a double-ring infiltrometer and Guelph permeameter had similar geometric means but the Guelph permeameter had greater variability than the double-ring infiltrometer.

An estimate of K_{sat} at each location was found using the mini disk infiltrometer, which resulted in a failure rate (FR) of 0%. The double-ring infiltrometer had a FR of 9.4%, and the Guelph permeameter had the highest FR at 15.6%. This higher FR is the result of several locations where a steady-state rate of flow was not achieved.

Employing a negative pressure and testing at a smaller scale, the mini disk infiltrometer determines the K_{sat} of the till matrix or fine-grained fraction. While the mini disk infiltrometer obtained more consistent estimates, this method underestimates hydraulic conductivity by failing to incorporate the till's coarse fraction when measuring K_{sat} . Since the mini disk infiltrometer measures the hydraulic conductivity of the fine fraction, this underestimation of K_{sat} indicates the dependency measurement scale has on hydraulic estimates.

Similarities in results between the double-ring infiltrometer and the Guelph permeameter suggest that the two methods have a comparable measurement scale, which accounts for the heterogeneity of the till (i.e., a variety of grain sizes are incorporated into the measured volume). FR and CV values for the double-ring infiltrometer and Guelph permeameter indicate that when measuring K_{sat} in highly heterogeneous sediment the

double-ring infiltrometer requires fewer measurements and obtains more reliable estimates of K_{sat} than the Guelph permeameter. This is consistent with the observations published by Gupta et al., (1993), where the number of measurements necessary for the Guelph permeameter to obtain estimated mean K_{sat} with comparable standard error to double-ring infiltrometer was higher. The similar results from the double-ring infiltrometer and Guelph permeameter also indicate that measurement methods conducted at the surface and at depth are equally effective. While some soil has developed on the glacial deposits the double-ring infiltrometer is not affected by this minimal soil and is an effective method for measuring the K_{sat} of till sediment.

5.4 Estimation of Groundwater Recharge

5.4.1 Snow Depth

Figure 5.4 presents the simulated daily snowpack depletion results for a north and south facing 7.5° slope, which was a representative average slope calculated from the land-surface topography (Figure 4.1). Using the measured wind speeds and assuming no additional precipitation input after April 20th, the model indicates the snowpack would take approximately 32 days to melt. Based on this initial sensitivity analysis the model shows little sensitivity to changes in land surface gradient and is slightly sensitive to aspect angle.

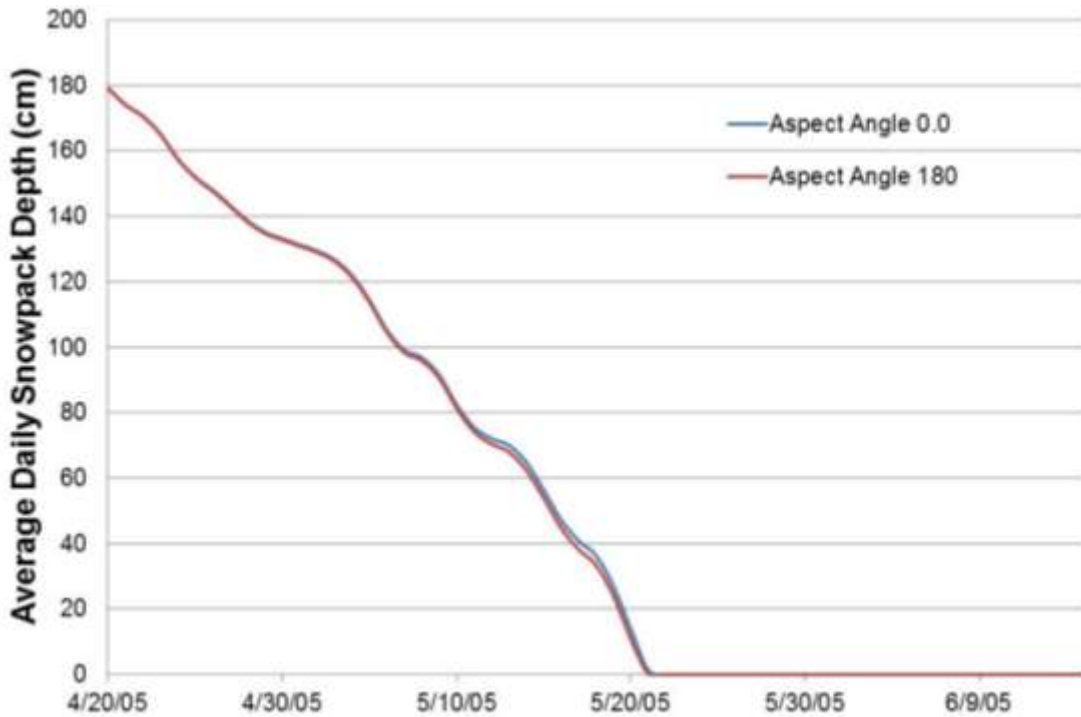


Figure 5.4: Simulated daily snow depths on north and south facing slopes at GLEES.

5.4.2 Modeled Ground Temperature and Soil Water Content

Simulated average daily ground temperatures at each depth for a 7.5° North and South facing slopes within GLEES are plotted in Figure 5.5a and b. Based on daily air temperature data and assumed sediment parameters, simulated temperatures respond to K_{sat} , snowpack depth, land surface gradient, and aspect angle. For the duration of each simulation the sediment remains unfrozen, but while the snowpack covers the sediment surface, temperatures remain between 0 and 5°C. Temperatures within the upper layers of the sediment column begin to increase reflecting daily temperature oscillations when snowpack depth reaches approximately 10 cm after May 20. Simulations show that ground temperatures are most influenced by aspect angle, rather than land surface

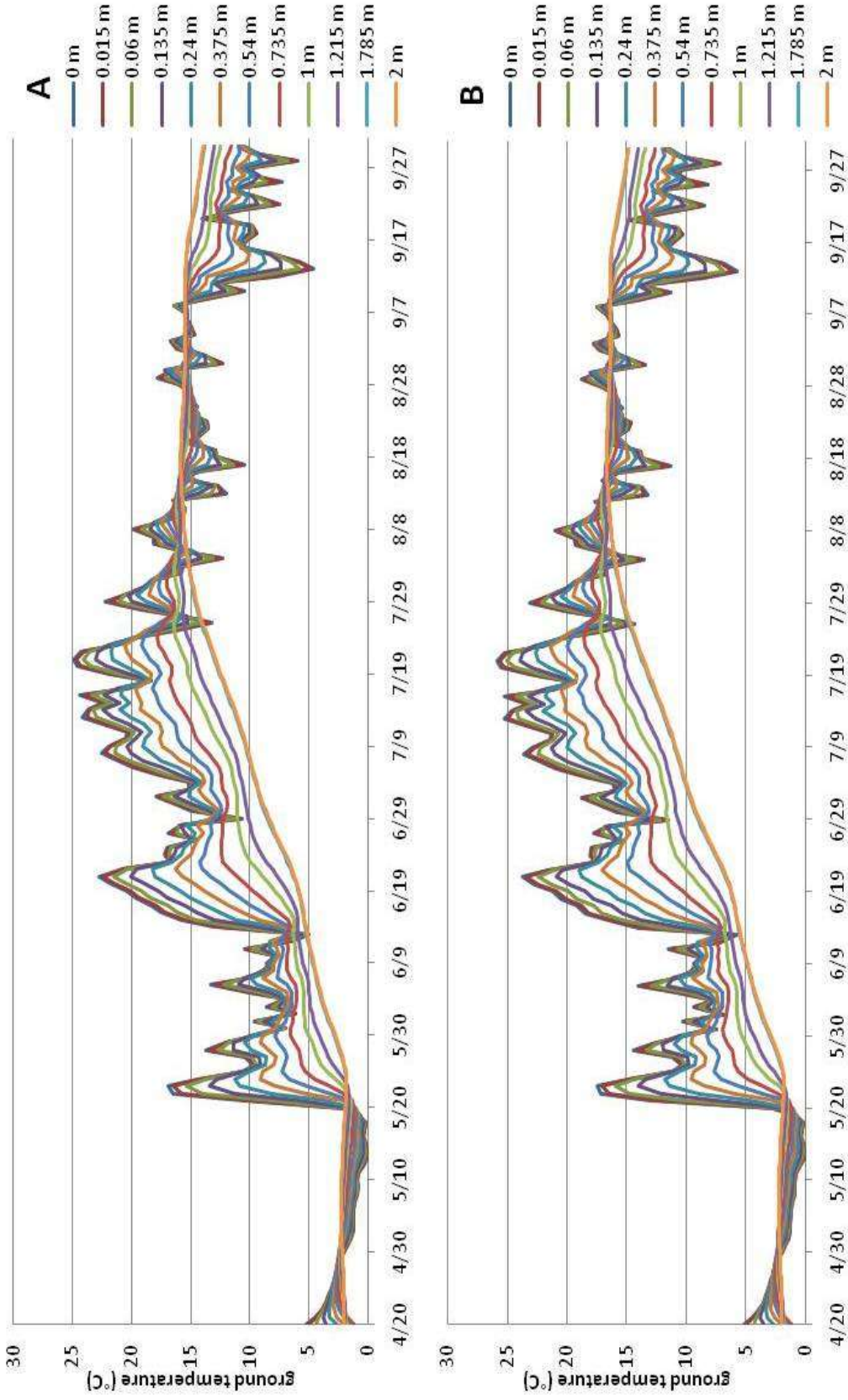


Figure 5.5: Simulated average daily ground temperatures during model runs on a 7.5° North (A) and South (B) facing slope using the double-ring infiltrometer geometric mean hydraulic conductivity.

gradient and K_{sat} . Based on the simulated ground temperatures the model is operating as expected with south facing slopes melting faster than north facing ones.

Simulated moisture contents are presented in Figures 5.6a-d through 5.9a-d. At the sediment surface the peaks and valleys of the simulated soil moisture content reflect modeled snow depth (Figure 5.10). In both models the sediment soil moisture contents at the surface peaks on May 20th when the snowpack disappears entirely, but in models using the large scale K_{sat} the peak is lower than scenarios using the small scale K_{sat} . Following this soil moisture peak, the sediment begins to drain at a rate controlled by the K_{sat} . Using the geometric mean K_{sat} values for the double-ring and mini disk infiltrometers, the scenario in which the more representative K_{sat} of 2.0×10^{-3} cm/sec is used indicates that the hydraulic conductivity is able to drain the sediment at a much faster rate than the melt rate preventing full saturation from occurring. The higher peak resulting from the scenario with the lower K_{sat} of 2.4×10^{-4} cm/sec indicates that draining will occur but over a much longer period.

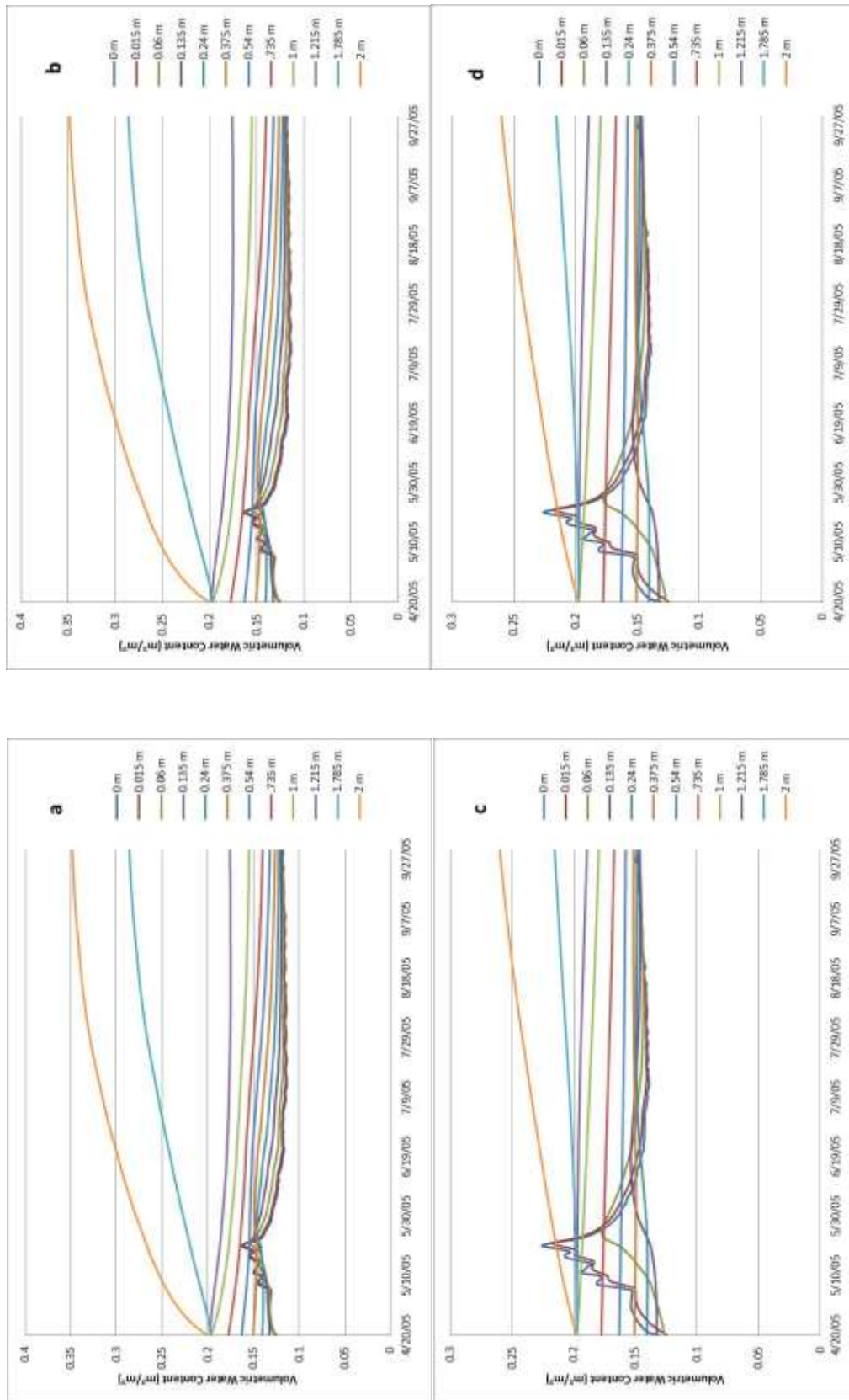


Figure 5.6: Sediment moisture changes at twelve depths using a land surface gradient of 0.1°. **a and b)** use the double-ring infiltrometer mean K_{sat} and are at the respective aspect angles of 0.0° and 180.0°. **c and d)** use the mini disk infiltrometer mean K_{sat} and are at the respective aspect angles of 0.0° and 180.0°.

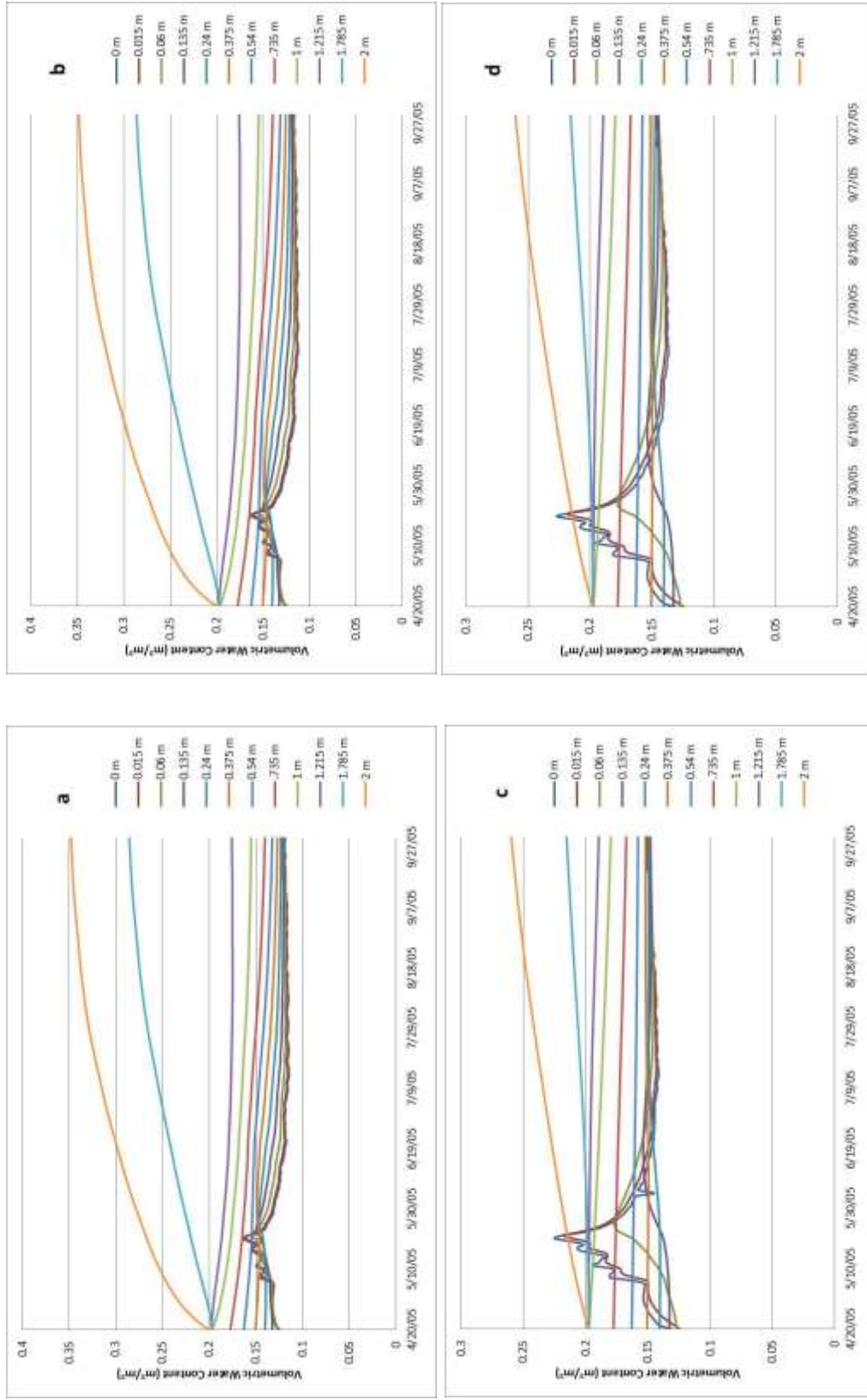


Figure 5.7: Sediment moisture changes at twelve depths using a land surface gradient of 7.5°. **a and b)** use the double-ring infiltrometer mean K_{sat} and are at the respective aspect angles of 0.0° and 180.0°. **c and d)** use the mini disk infiltrometer mean K_{sat} and are at the respective aspect angles of 0.0° and 180.0°.

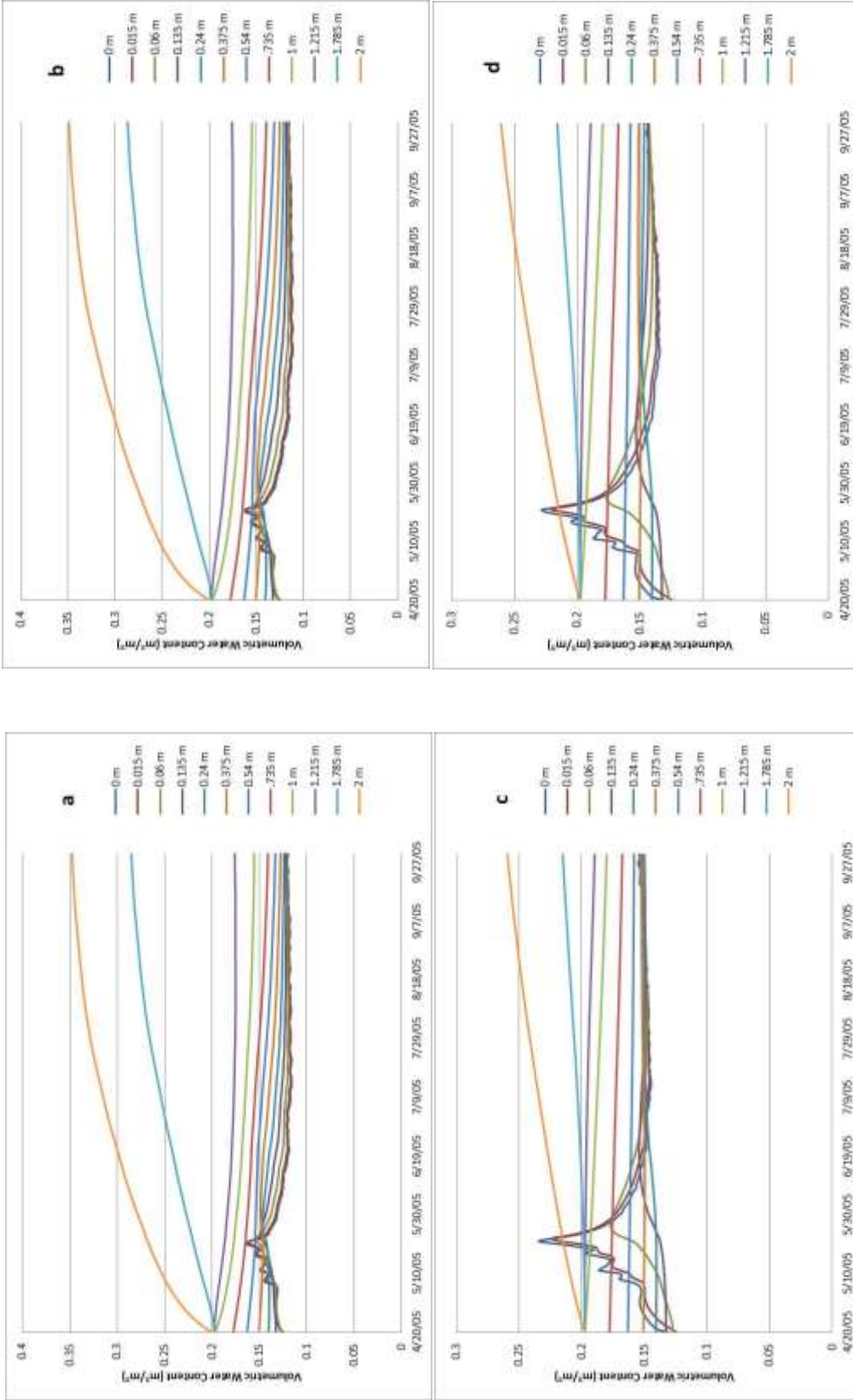


Figure 5.8: Sediment moisture changes at twelve depths using a land surface gradient of 15° : **a and b**) use the double-ring infiltrometer mean K_{sat} and are at the respective aspect angles of 0.0° and 180.0° . **c and d**) use the mini disk infiltrometer mean K_{sat} and are at the respective aspect angles of 0.0° and 180.0° .

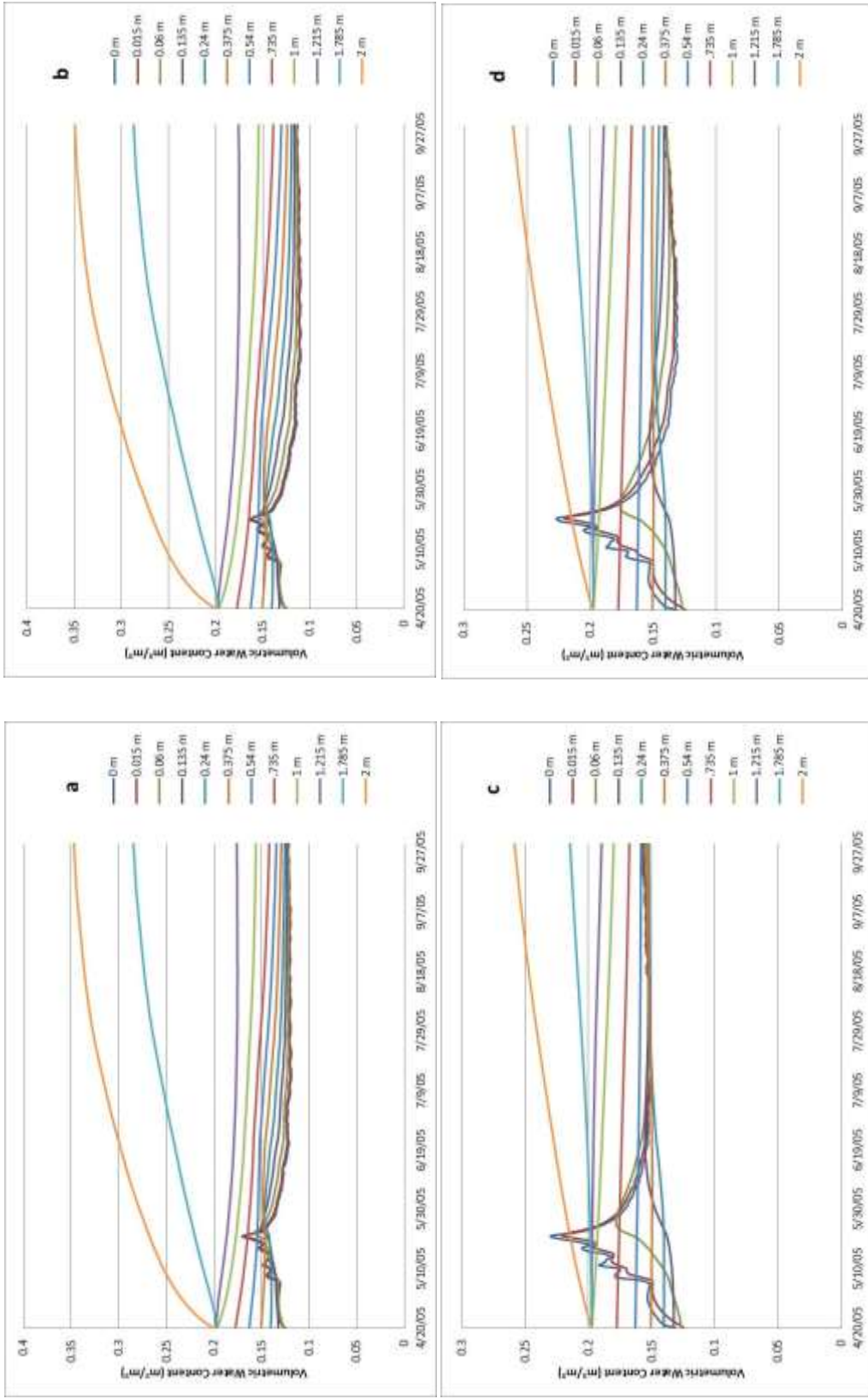


Figure 5.9: Sediment moisture changes at twelve depths using a land surface gradient of 29.5°. **a and b)** use the double-ring infiltrometer mean K_{sat} and are at the respective aspect angles of 0.0° and 180.0°. **c and d)** use the mini disk infiltrometer mean K_{sat} and are at the respective aspect angles of 0.0° and 180.0°.

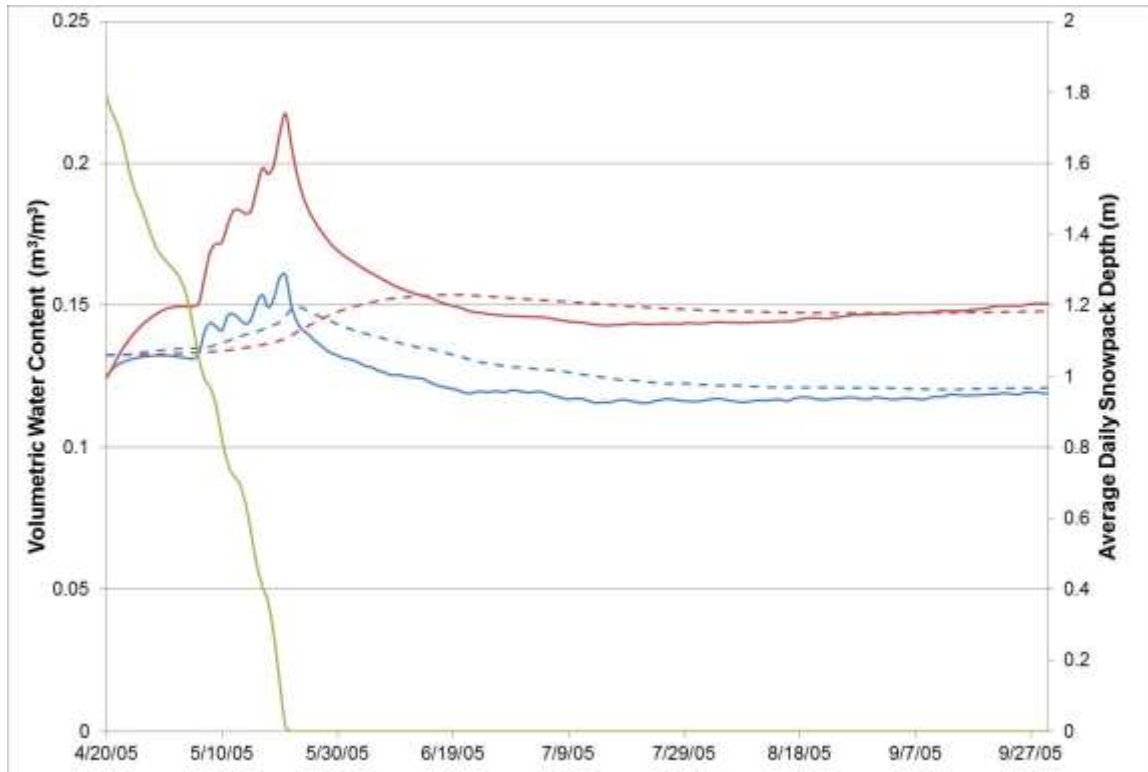


Figure 5.10: Simulated snow depth and surface moisture contents plotted to show the timing of the sediment moisture changes in response to melting events. The red lines are simulations using the small scale (mini disk infiltrometer) K_{sat} values, the blue lines are from simulations using the large scale (double-ring infiltrometer) K_{sat} values, blue and red solid lines are volumetric water contents at 1.5 cm depth and dashed lines are 13.5 cm deep. The green line is the simulated average daily snowpack depth. This plot was created using the 7.5° land surface gradient scenario.

As described in section 4.4.2, model-simulated flow through the subsurface interval from 1.785 m to 2 m below ground surface was calculated in order to quantify groundwater recharge. Calculated daily flow rates through this 0.215 m³ sediment volume are shown in Figure 5.11. Calculated flow rates support the observation that sediments using the more representative K_{sat} estimated with the double-ring infiltrometer will drain faster than the lower K_{sat} provided by the mini disk infiltrometer. Sensitivity to slope angle was evaluated and did not have a significant effect. Simulations using the

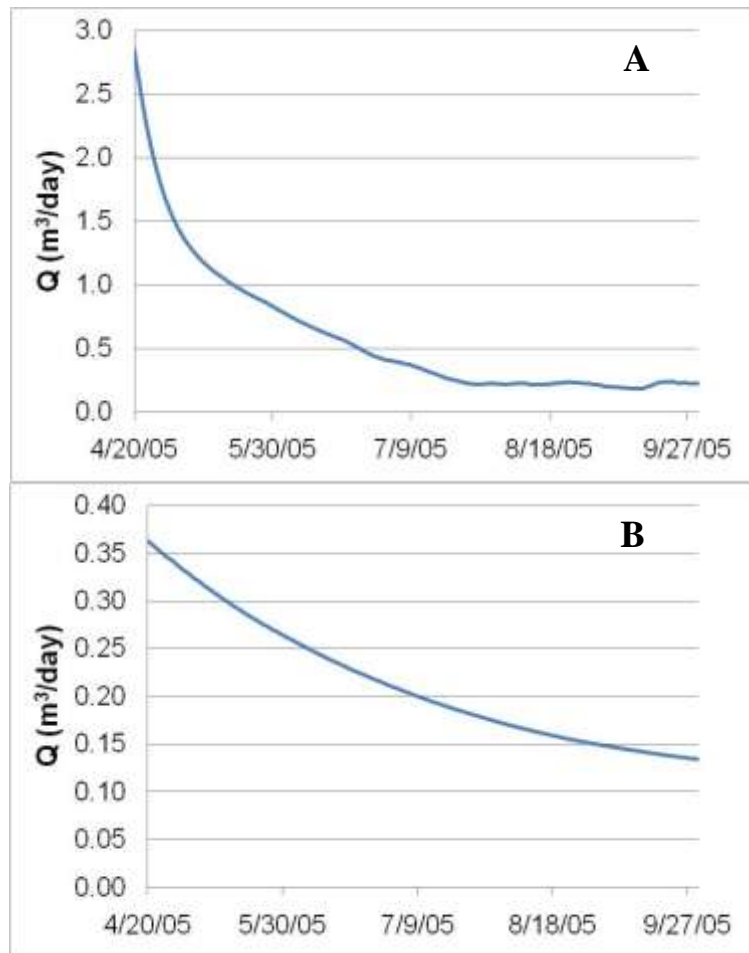


Figure 5.11: Calculated daily vertical flow rate at a depth of 2 m using K_{sat} values estimated from the larger scale measurements (A) and small scale measurements (B).

two K_{sat} values also show that in areas where the K_{sat} is higher, the sediment will achieve a constant rate of flow before low K_{sat} sediments. In areas where the K_{sat} is high there will be greater amounts of recharge. Based on the simulated estimates of sediment moisture contents the total volume of water flowing vertically towards the water table in the high K_{sat} scenario is nearly three times that of the low K_{sat} scenario. This means that the sediments with lower field-saturated hydraulic conductivity retain more of the water than sediments with higher values.

CHAPTER 6

6. CONCLUSIONS

Three different measurement techniques (mini disk infiltrometer, double-ring infiltrometer, and Guelph permeameter) were used to measure field-saturated hydraulic conductivity (K_{sat}) of alpine glacial till at Glacial Lakes Ecosystem Experiments Site in southern Wyoming. Mean K_{sat} values obtained with the mini disk infiltrometer, the double-ring infiltrometer, and Guelph permeameter were 0.014 cm/min, 0.12 cm/min, and 0.094 cm/min, respectively.

The results from the method comparison indicate that when measuring K_{sat} in sediments containing a wide mixture of particle sizes, measurement scale must be considered. Measured hydraulic conductivities with the double-ring infiltrometer and Guelph permeameter are consistently higher than the mini disk infiltrometer. Having a similar measurement scale these methods measure K_{sat} at a larger scale which incorporates the extreme mixture of particle sizes that make up the till. The mini disk infiltrometer, having a smaller measurement scale, obtains the K_{sat} of the fine-grained fraction. When measuring K_{sat} in material with a high coarse fraction a method must be chosen that integrates the coarse fraction, making small-scale measurement techniques such as the mini disk infiltrometer ineffective. The similarities between the means and ranges of K_{sat} values obtained by the double-ring infiltrometer and Guelph permeameter also indicates that, in areas with minimal soil development, measurements of hydraulic

conductivity taken at the sediment surface are representative of the hydrogeologic properties at depth and can be used when considering subsurface groundwater flow.

To evaluate the implications measurement scale has groundwater recharge, a physically-based one-dimensional model was used to consider the hydraulic response in the watershed during snowmelt. Using the geometric mean hydraulic conductivity values obtained with the double-ring and mini disk infiltrometers and available snowpack data from the 2005 water year, FASST was able to simulate snowpack depletion and soil moisture changes. Based on the groundwater discharge volumes calculated for each hydraulic conductivity scenario, the small measurement scale of the mini disk infiltrometer will tend underestimate recharge. Calculations also show that when the more realistic (larger scale) hydraulic conductivity is used, the sediment drains and returns to a steady-state rate of flow relatively quickly. With a lower hydraulic conductivity (the mean hydraulic conductivity from the mini disk infiltrometer measurements) the sediment will continue to drain throughout the year, never achieving steady-state flow. These calculations and simulations demonstrate the importance of accurately characterizing the hydraulic conductivity of alpine glacial sediments.

CHAPTER 7

7. RECOMMENDATIONS FOR FUTURE WORK

This study which characterizes the hydrogeologic properties of the glacial till at GLEES and examines the scale dependency of groundwater recharge has revealed numerous avenues for future work. Some of these include:

- Further evaluate the effectiveness of each hydraulic conductivity measurement method in other mountain watersheds with surficial glacial till.
- Improve accuracy of the snowmelt/soil moisture model by considering additional precipitation after model initialization and by incorporating additional detail on the multiple processes that influence snowpack depletion.
- Install piezometers and use site-specific water level measurements to calibrate numerical model simulations and refine estimates of groundwater recharge.
- Incorporate this work into a new water balance assessment to better understand the hydrology at Glacial Lakes Ecosystem Experiments Site and other similar watersheds.

CHAPTER 8

LITERATURE CITED

- ASTM Standard D 422-63, 2007. "Standard Test Method for Particle-Size Analysis of Soils," ASTM International, West Conshohocken, PA, 2007, DOI: 10.1520/D0422-63R07, www.astm.org.
- ASTM Standard D 3385, 2003. "Standard Test Method for Infiltration Rate of Soils in Field Using Double-Ring Infiltrometer," ASTM International, West Conshohocken, PA, 2003, DOI: 04.08/D3385-03, www.astm.org.
- ASTM Standard D 5126-90, 2004. "Standard Guide for Comparison of Field Methods for Determining Hydraulic Conductivity in Vadose Zone," ASTM International, West Conshohocken, PA, 2004, www.astm.org.
- Bagarello, V. and G. Provenzano, 1996. Factors Affecting Field and Laboratory Measurement of Saturated Hydraulic Conductivity. *Transactions of the ASAE*, 39:153-159.
- Bagarello, V., 1997. Influence of Well Preparation on Field-Saturated Hydraulic Conductivity Measured With the Guelph Permeameter. *Geoderma*, 80, 169-180.
- Bagarello, V., S. Sferlazza, and A. Sgroi, 2009. Comparing Two Methods of Analysis of Single-Ring Infiltrometer Data for a Sandy-Loam Soil. *Geoderma*, 149: 415-420.
- Bouma, J., 1983. Use of Soil Survey Data to Select Measurement Techniques for Hydraulic Conductivity. *Agricultural Water Management*, 6, 177-190.
- Bouwer, H. and R.C. Rice, 1984. Hydraulic Properties of Stony Vadose Zones. *Ground Water*, 22 (6), 696-705.
- Bouwer, H., 1986. *Intake Rate: Cylinder Infiltrometer*, in *Methods of Soil Analysis, Part 1: Physical and Mineralogical Methods*, Agronomy Monograph No. 9, American Society of Agronomy, Madison, WI, 825-844 pp.
- Brakensiek, D.L., W.J. Rawls, and G.R. Stephenson, 1986. Determining the saturated hydraulic conductivity of a soil containing rock fragments. *Soil Science Society of America Journal*, 50, 834-835.

- Brakensiek, D.L., and W.J. Rawls, 1994. Soil Containing Rock Fragments: Effects on Infiltration. *Catena*, 23, 99–110.
- Brock, B.W., I.C. Willis, and M.J. Sharp, 2006. Measurement and Parameterization of Aerodynamic Roughness Length Variations at Haut Glacier d’Arolla, Switzerland. *Journal of Glaciology*, 52, 281-297, doi: 10.3189/172756506781828746.
- Cheng, Q., X. Chen, X. Chen, Z. Zhang, and M. Ling, 2011. Water infiltration underneath single-ring permeameters and hydraulic conductivity determination. *Journal of Hydrology*, 398, 135-143.
- Day, C. A., 2009. Modelling Impacts of Climate Change on Snowmelt Runoff Generation and Streamflow Across Western US Mountain Basins: A Review of Techniques and Applications for Water Resource Management. *Progress in Physical Geography*, 33 (5), 614-633.
- DeBeer, C. M. and J. W. Pomeroy, 2009. Modelling Snow Melt and Snowcover Depletion in a Small Alpine Cirque, Canadian Rocky Mountains. *Hydrological Process*, 23, 2584-2599.
- DeBeer, C. M. and J. W. Pomeroy, 2010. Simulation of the Snowmelt Runoff Contributing Area in a Small Alpine Basin. *Hydrol. Earth Syst. Sci.*, 14, 1205-1219.
- Decagon Devices, Inc., 2007. *Mini Disk Infiltrometer, User’s Manual Version 6*, Decagon Devices, Inc., Pullman, WA.
- Fies, J., N. De Louvigny, and A. Chanzy, 2002. The Role of Stones in Soil Water Retention. *European Journal of Soil Science*, 53, 95-104.
- Frankenstein, S. and G. Koenig, 2004. *Fast All-season Soil Strength (FASST)*. ERDC/CRREL Special Report SR-04-1, 107 pp.
- Frankenstein, S., A. Sawyer, and J. Koeberle, 2008. Comparison of FASST and SNTHERM in three snow accumulation regimes. *Journal of Hydrometeorology*, 9, 1443-1463, DOI: 10.1175/2008JHM865.1
- Gee, G.W. and J.W. Bauder, 1986. Chapter 15 “Particle-Size Analysis” in *Methods of Soil Analysis, Part 1. Physical and Mineralogical Methods*, Second Ed., edited by A. Klute, Soil Sci. Soc. Am., Madison, WI, 1188 pp.
- Gupta, R.K., R. P. Rudra, W.T. Dickinson, N.K. Patni, and G.J. Wall, 1993. Comparison of Saturated Hydraulic Conductivity Measured by Various Field Methods. *American Society of Agricultural Engineers*, 36: 51-55.

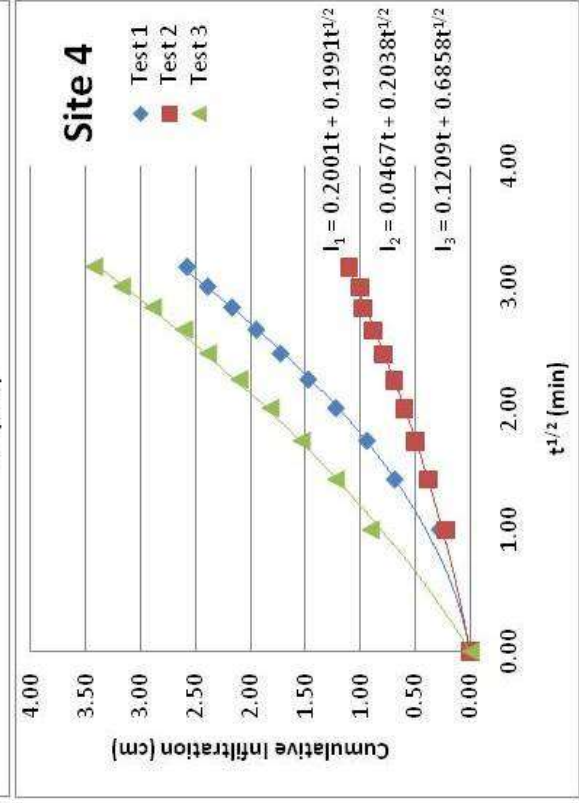
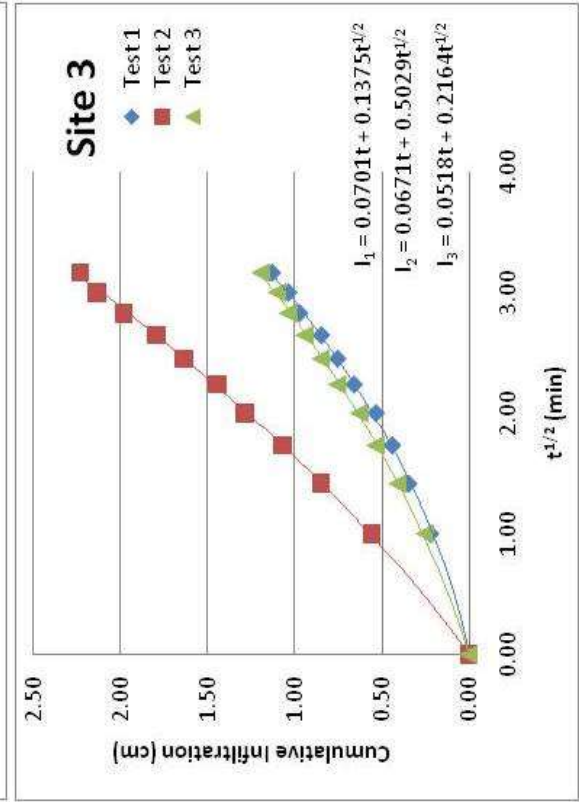
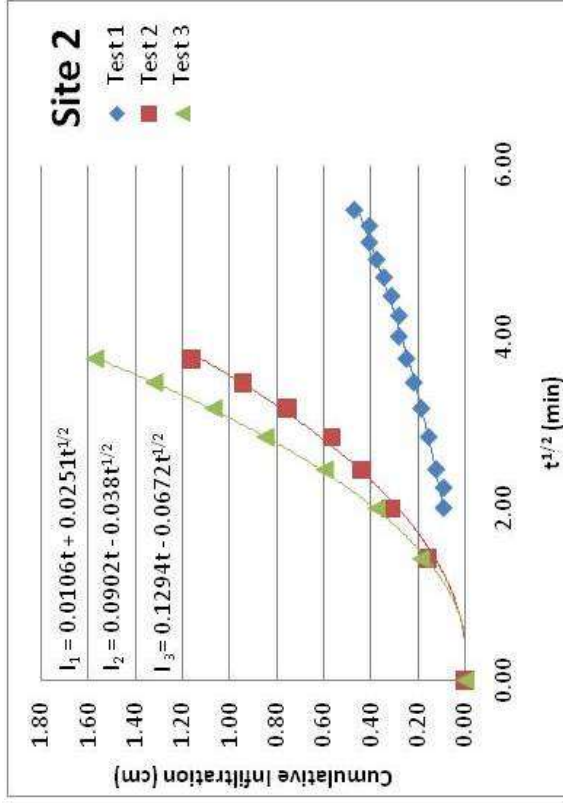
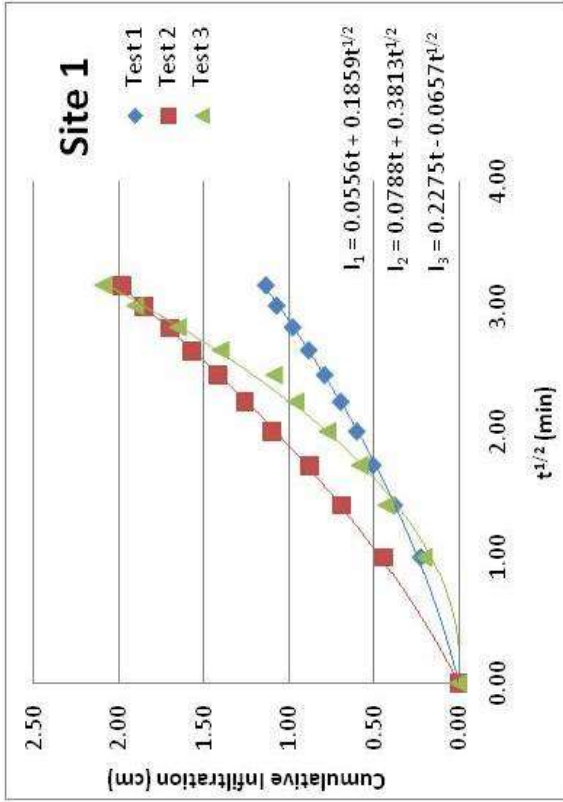
- Gupta, N., R. P. Rudra, and G. Parkin, 2006. Analysis of Spatial Variability of Hydraulic Conductivity at Field Scale. *Canadian Biosystems Engineering*, 48, 1.55-1.62.
- Healy, R.W., T.C. Winter, J.W. LaBaugh, and O.L. Franke, 2007. Water Budgets: Foundations for Effective Water-Resources and Environmental Management. *U.S. Geological Survey Circular 1308*, 90 pp.
- Holcombe, J., 2004. *A Modeling Approach to Estimating Snow Cover Depletion and Soil Moisture Recharge in a Semi-Arid Climate at Two NASA CLPX Sites*. Master of Science Thesis, Department of Forest, Rangeland and Watershed Stewardship, Colorado State University, Fort Collins, Colorado, 104 pp.
- Hopper, R.E., and P.M. Walthall, 1994. Chapter 5 "Soils" in *The Glacier Lakes Ecosystem Experiments Site*, R.C. Musselman (editor), General Technical Report RM-249.
- Hultstrand, D., 2006. *Geostatistical Methods for Estimating Snowmelt Contribution to the Seasonal Water Balance in an Alpine Watershed*. Master of Science Thesis, Department of Forest, Rangeland and Watershed Stewardship, Dept. of Forest, Rangeland, and Watershed Stewardship, Colorado State University, Fort Collins, Colorado, 117 pp.
- Jensen, P. D., 1990. Methods for Measuring the Saturated Hydraulic Conductivity of Tills. *Nordic Hydrology*, 21, 95-106.
- Jordan, R., 1991. *A One-Dimensional Temperature Model for a Snow Cover*. ERDC/CRREL Special Report 91-16, 49 pp.
- Kanwar, R.S., H.A. Rizvi, M. Ahmed, R. Horton, and S.J. Marley, 1989. Measurement of Field-Saturated Hydraulic Conductivity by Using Guelph and Velocity Permeameters, *American Society of Agricultural Engineers*, 32, 1885-1890.
- Korfmacher, J.L. and D.M. Hultstrand, 2006. Glacier Lakes Ecosystem Experiments Site hourly meteorology tower data. Fort Collins, CO: U.S. Department of Agriculture, Forest Service, Rocky Mountain Research Station.
- Lee, D.M., W.D. Reynolds, D.E. Eldrick, and B.E. Clothier, 1985. A Comparison of Three Field Methods for Measuring Saturated Hydraulic Conductivity. *Can. J. Soil Sci.*, 65, 563-573.
- Ma, D.H. and M.G. Shao, 2008. Simulating Infiltration into Stony Soils with a Dual-Porosity Model. *European Journal of Soil Science*, 59, 950-959.
- Mehuys, G.R., L.H. Stolzy, J. Letey, and L.V. Weeks, 1975. Effect of Stones on the Hydraulic Conductivity of Relatively Dry Desert Soils. *Soil Science Society of America Proc.*, 39, 37-42.

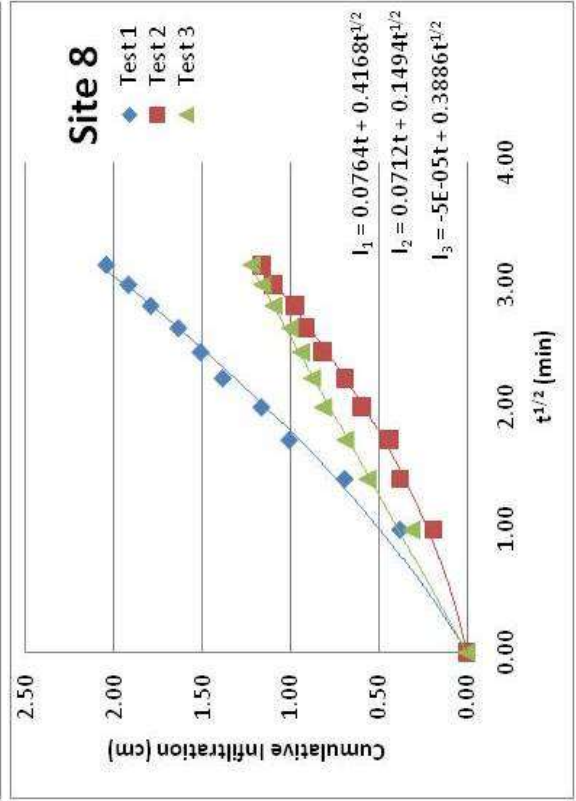
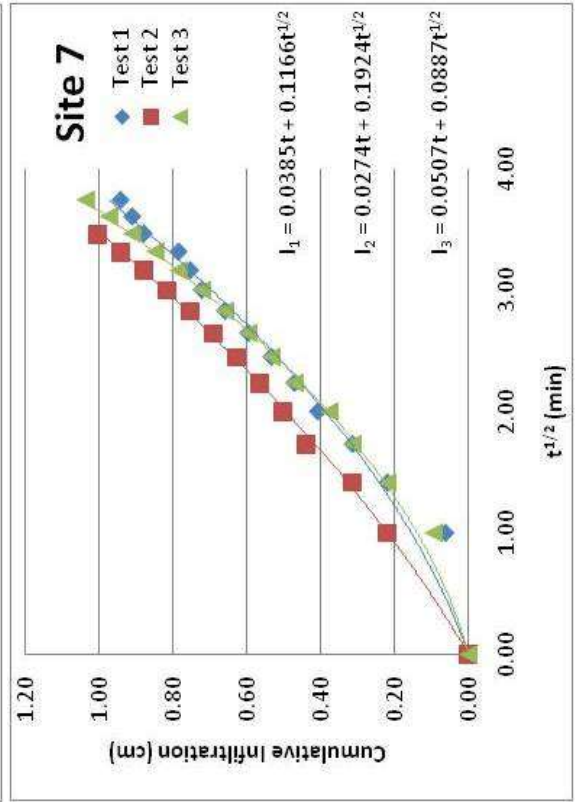
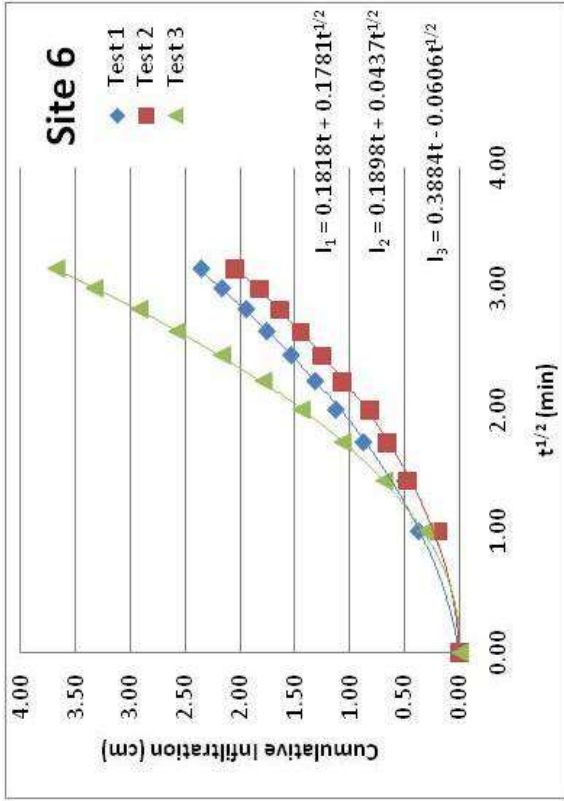
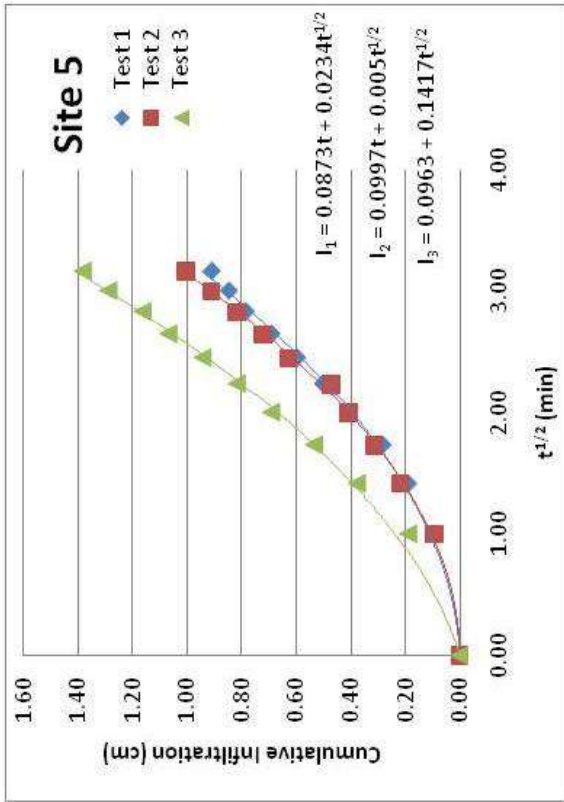
- Mohanty, B., R. Kanwar, and C. Everts, 1994. Comparison of Saturated Hydraulic Conductivity Measurement Methods for a Glacial-Till Soil. *Soil Sci. Soc. Am.*, 58, 672-677.
- Musselman, R.C., 1994. The Glacier Lakes Ecosystem Experiments Site, *Rocky Mountain Forest and Range Experiment Station, General Technical Report RM-249*, 94 pp.
- Page, N., 2011. *Application of ground penetrating radar to sub-alpine hydrogeology, Snowy Range, Wyoming*. Master of Science Thesis, Department of Geology, Colorado State University, Fort Collins, Colorado, 74 pp.
- Paige G. B. and D. Hillel, 1993. Comparisons of three methods for assessing soil hydraulic parameters. *Soil Science*, 155 (3), 176-189.
- Peck, A.J., and J.D. Watson. 1979. Hydraulic conductivity and flow in non-uniform soil. In Workshop on Soil Physics and Field Heterogeneity. CSIRO Division of Environmental Mechanics, Canberra, Australia.
- Poesen, J., and H. Lavee, 1994. Rock Fragments in Top Soils: Significance and Processes. *Catena*, 23, 1–28.
- Ravina, I., and J. Magier, 1984. Hydraulic Conductivity and Water Retention of Clay Soils Containing Coarse Fragments. *Soil Science Society of America Journal*, 48, 736–740.
- Rawls, W. J., L. R. Ahuja, D.L. Brakensiek, and A. Shirmohammadi, 1993. *Infiltration and Soil Water Movement*, in *Handbook of Hydrology*, edited by D. R. Maidment, McGraw-Hill, Inc., New York, 5.1-5.51 pp.
- Reynolds, W. D. and D. E. Elrick, 1986. A Method for Simultaneous In Situ Measurement in the Vadose Zone of Field-Saturated Hydraulic Conductivity, Sorptivity and the Conductivity-Pressure Head Relationship. *Ground Water Monitoring & Remediation*, 6, 84-95.
- Reynolds, W.D., 2008a. Chapter 76 “Saturated Hydraulic Properties: Well Permeameter” in *Soil Sampling and Methods of Analysis*, Second Edition, CRC Press, Boca Raton, FL, 1224 pp.
- Reynolds, W.D., 2008b. Chapter 77 “Saturated Hydraulic Properties: Ring Infiltrometer” in *Soil Sampling and Methods of Analysis*, Second Edition, CRC Press, Boca Raton, FL, 1224 pp.
- Rochette, E.A., 1994. Chapter 4 "Geology" in *The Glacier Lakes Ecosystem Experiments Site*, R.C. Musselman (editor), General Technical Report RM-249.

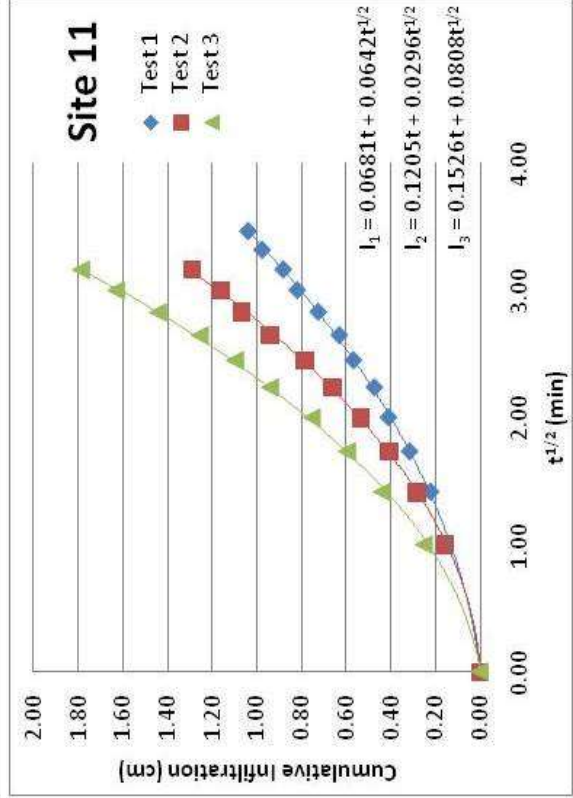
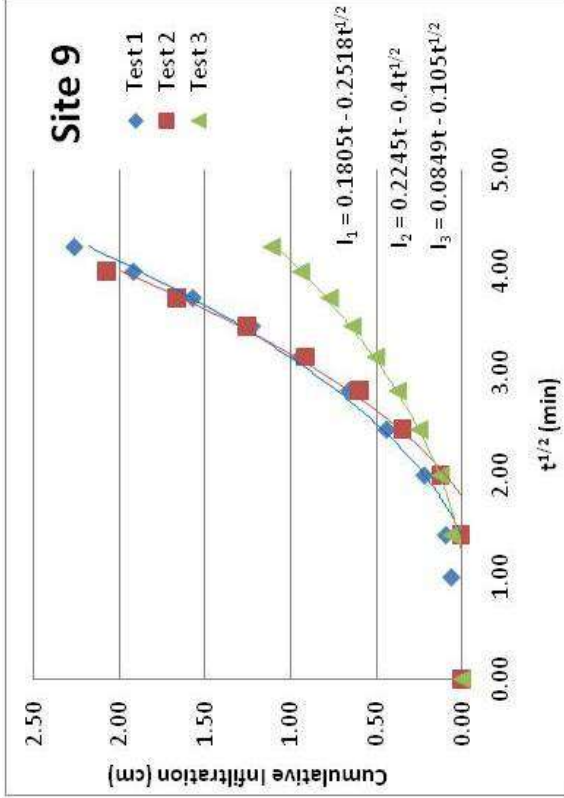
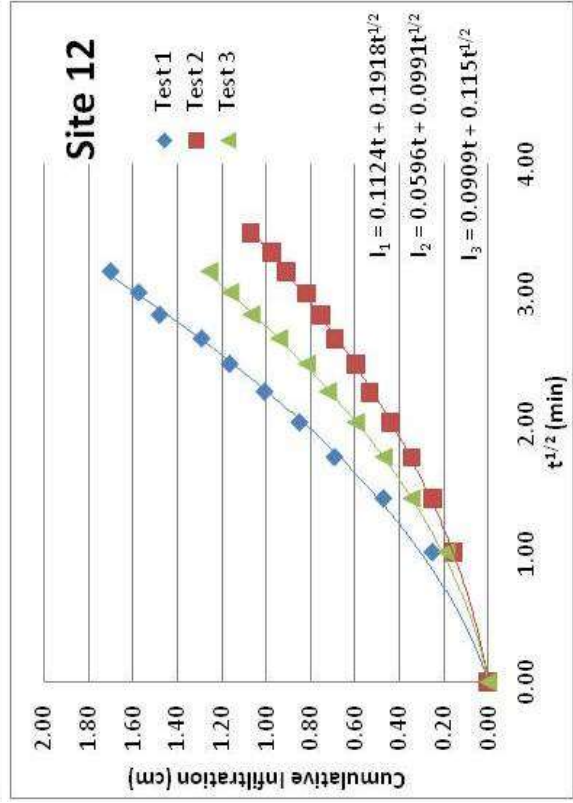
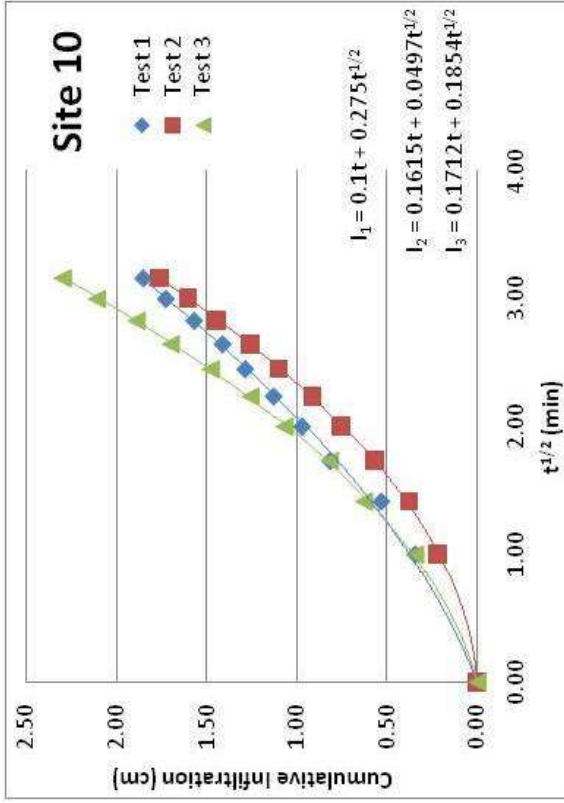
- SAS Institute Inc. 2010. *Statistical Analysis Software: Release 9.2*. SAS Campus Drive, Cary, North Carolina 27513, USA.
- Sauer, T. J., and S.D. Logsdon, 2002. Hydraulic and Physical Properties of Stony Soils in a Small Watershed, *Soil Science Society of America Journal*, 66, 1947-1956.
- Sawyer, A., 2007. *Snowpack Depletion Modeling using Fast All-Season Soil Strength (FASST) and Snowmodel in a High-Elevation, High Relief Catchment in the Central Rocky Mountains*, Master of Science Thesis, Department of Forest, Rangeland, and Watershed Stewardship, Colorado State University, Fort Collins, Colorado, 99 pp.
- Soil Moisture Equipment Corp., 2008. *2800K1 Operating Instructions*, Soil Moisture Equipment Corp., P.O. Box 30025, Santa Barbara, CA 93105, USA.
- Sommerfeld, R.A., 1994. Chapter 10 "Snow" in *The Glacier Lakes Ecosystem Experiments Site*, R.C. Musselman (editor), General Technical Report RM-249.
- Vanderlinden, K., D. Gabriels, and J.V. Giráldez, 1998. Evaluation of infiltration measurements under olive trees in Córdoba. *Soil & Tillage Research*, 48, 303-315.
- van Genuchten, M. Th., 1980. A Closed-Form Equation for Predicting the Hydraulic Conductivity of Unsaturated Soils. *Soil Science Society of America Journal*, 44, 892-898.
- Verbist, K., J. Baetens, W.M. Cornelis, D. Gabriels, C. Torres, and G. Soto, 2009. Hydraulic Conductivity as Influenced by Stoniness in Degraded Drylands of Chile. *Soil Science Society of America Journal*, 73, 471-484.
- Warrick, A.W. and D.R. Nielsen, 1980. *Spatial Variability; of Soil Physical Properties in the Field*. in *Applications of Soil Physics*. D. Hillel (editor), Academic Press, Toronto, Ont. 319-344 pp.
- Zhang, R., 1997. Determination of Soil Sorptivity and Hydraulic Conductivity from the Disk Infiltrimeter. *Soil Science Society of America Journal*, 61, 1024-1030.

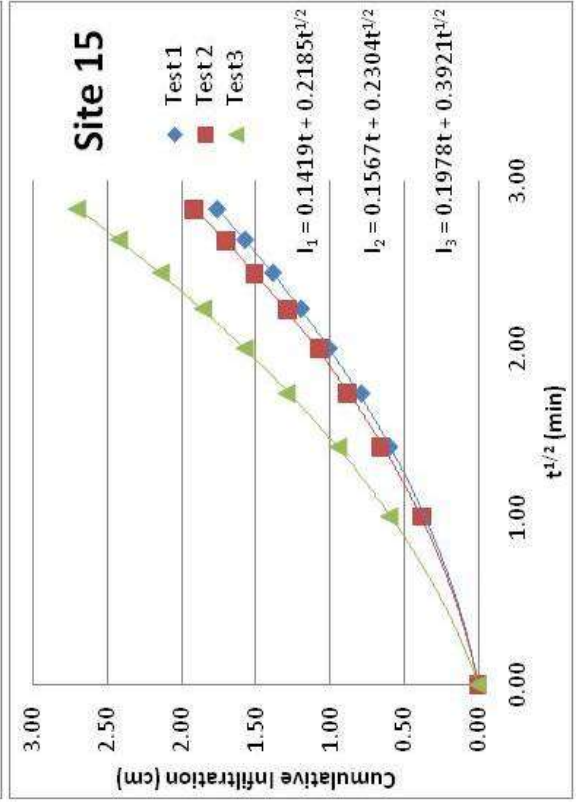
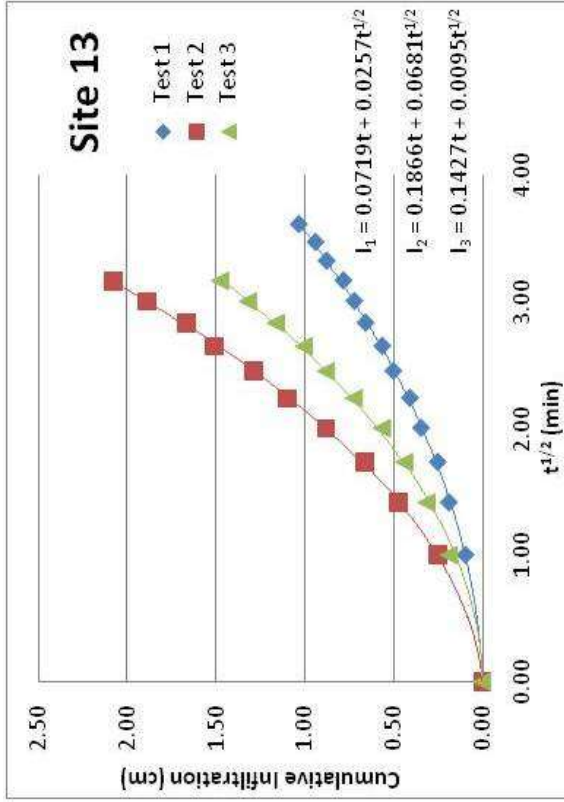
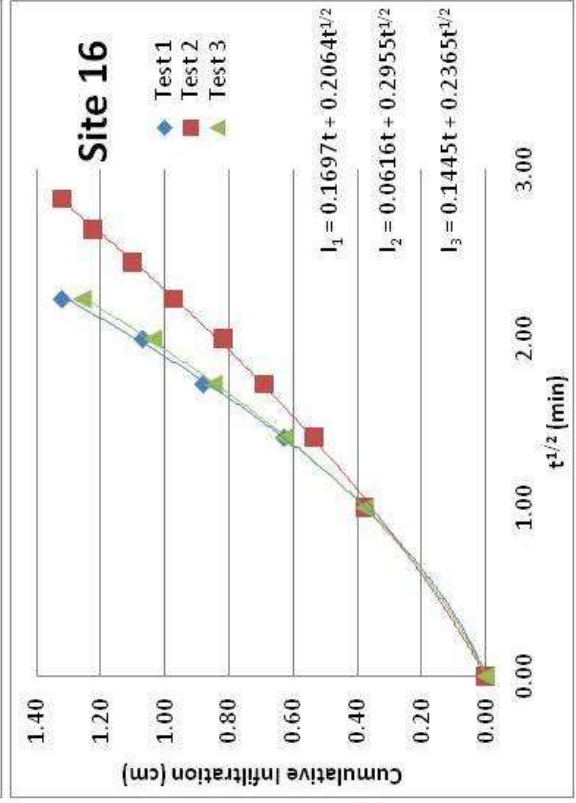
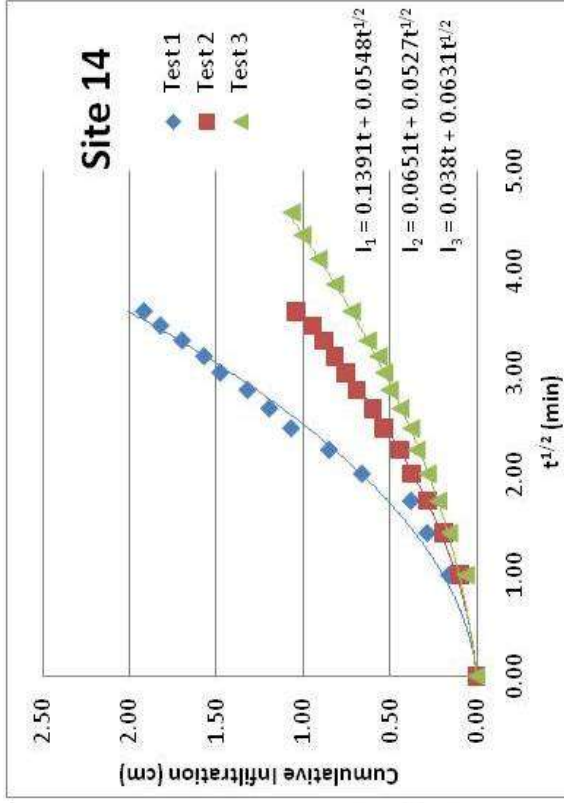
APPENDIX A

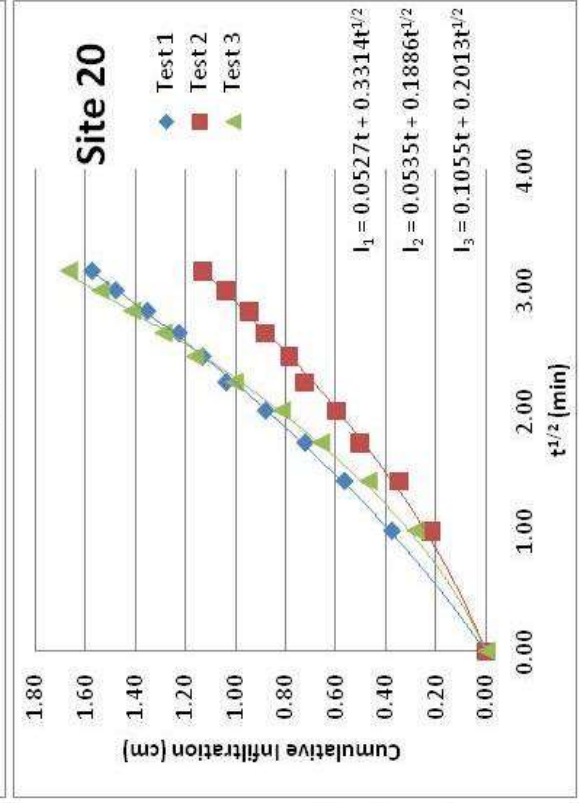
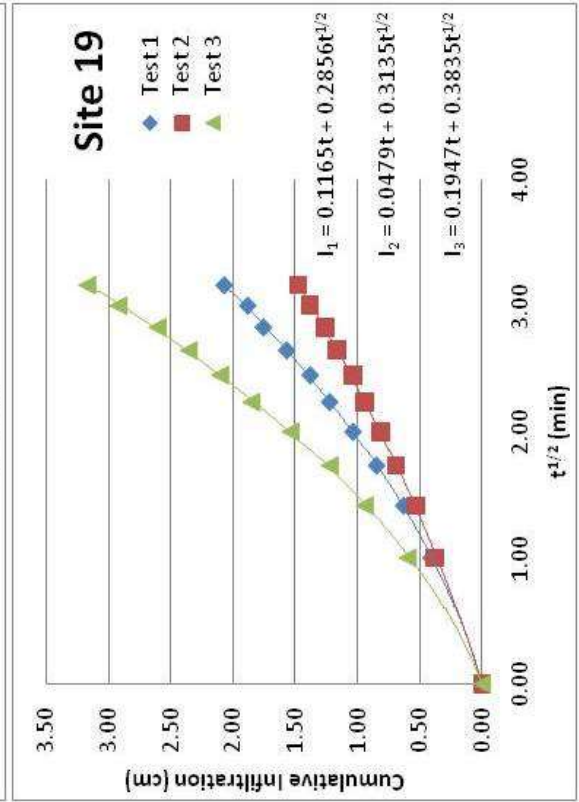
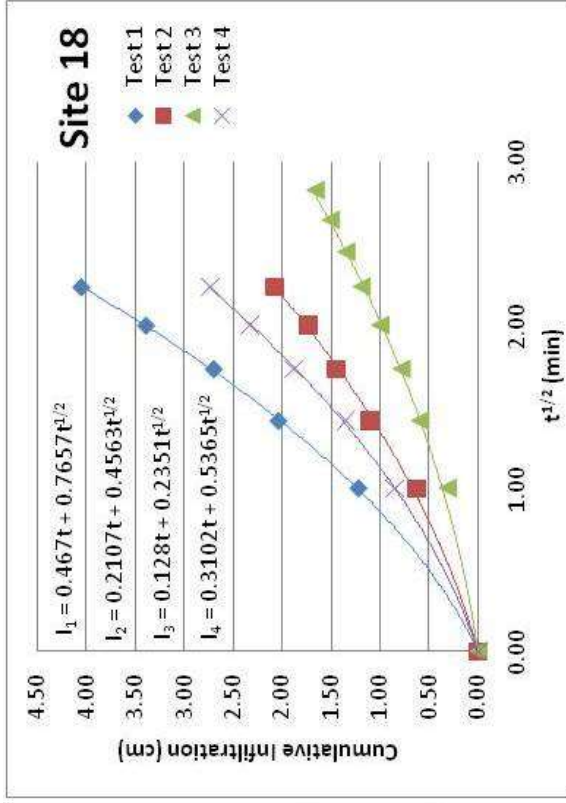
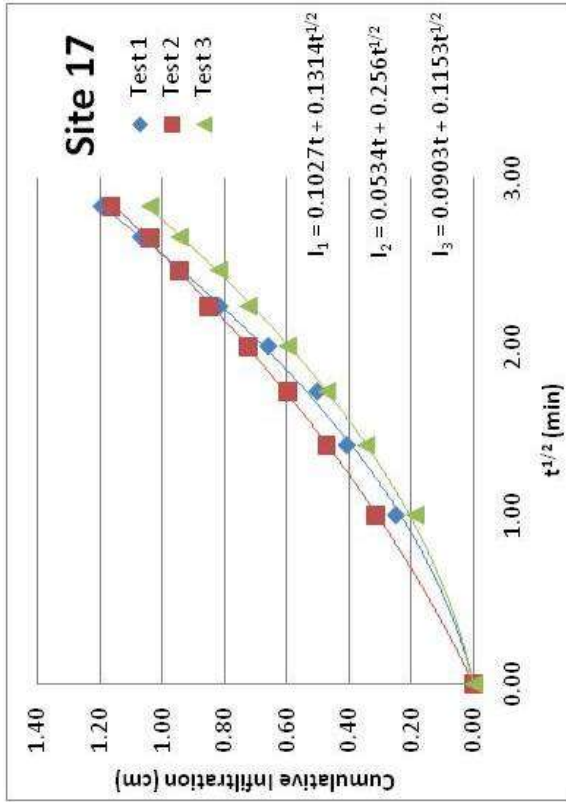
This appendix contains results from the mini disk infiltrometer tests. Three tests were conducted at each measurement location shown in Figure 4.1. The equations shown on the plots in this appendix give the best fit polynomial ($I = C_1t + C_2t^{1/2}$) for each infiltration test data set. As noted in chapter 4.1.1.2, the best fit C_1 coefficient is used to obtain the hydraulic conductivity value.

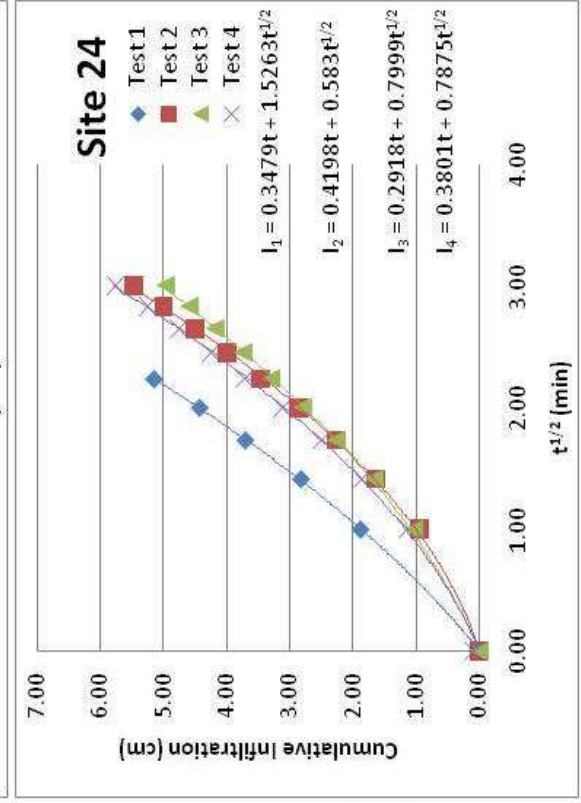
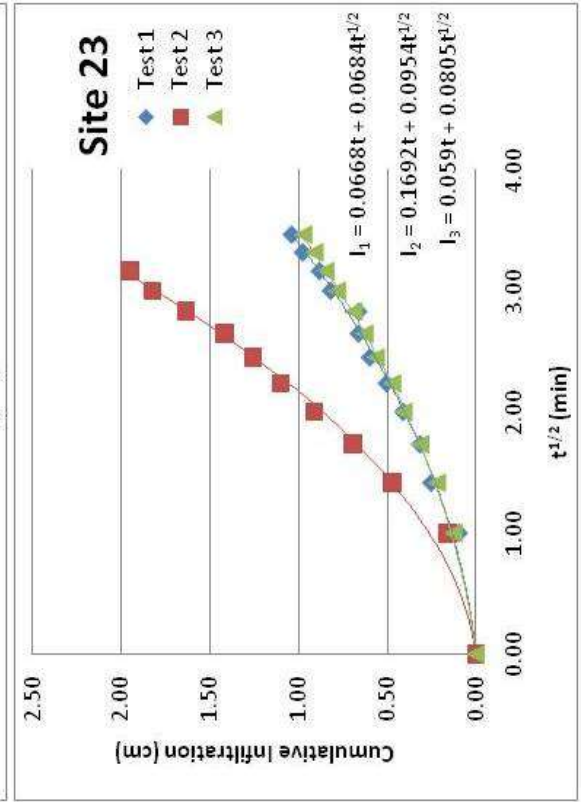
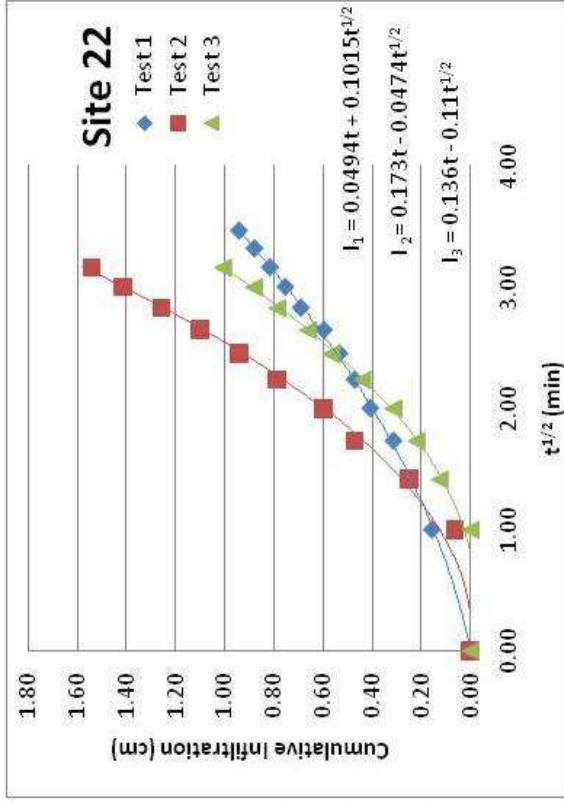
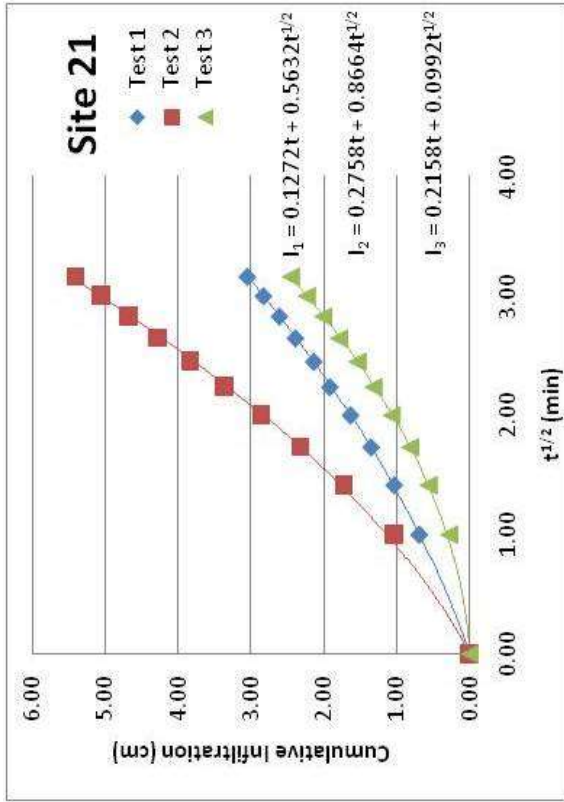


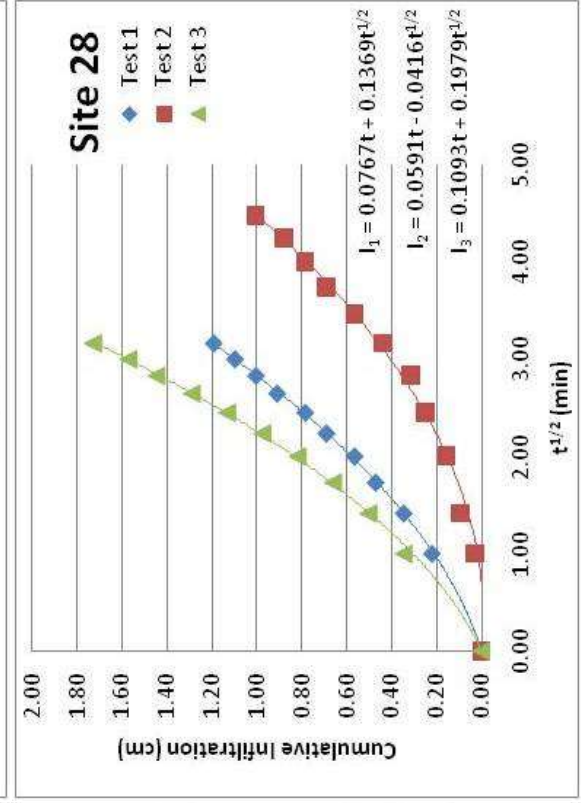
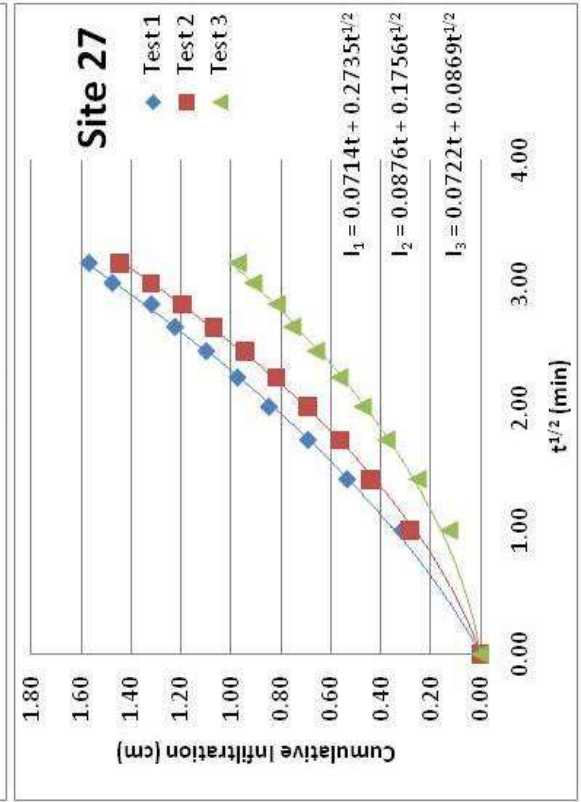
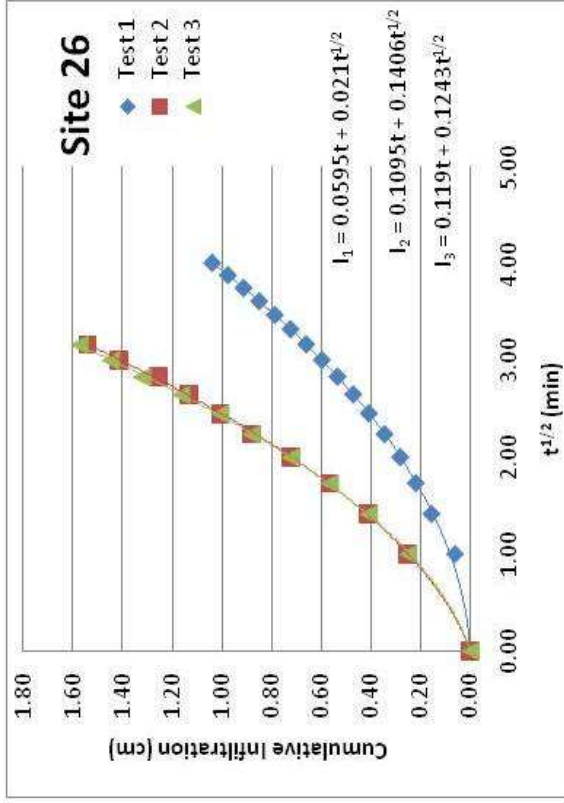
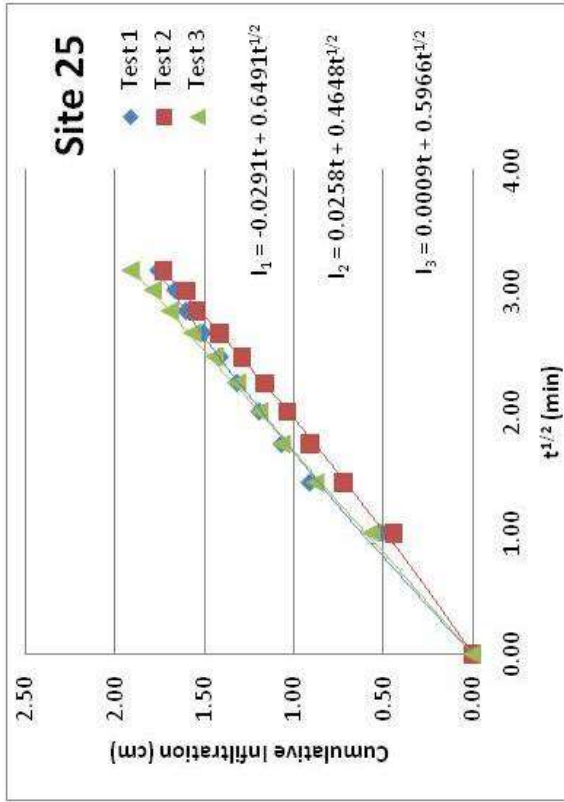


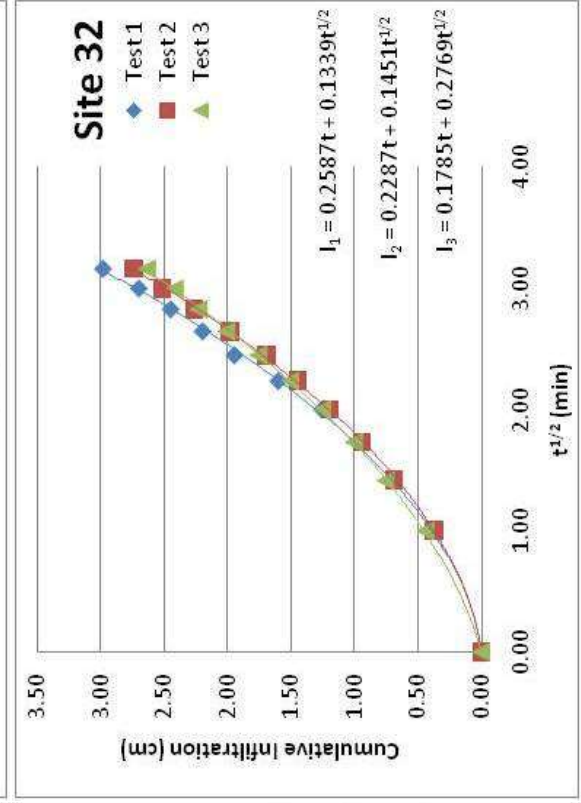
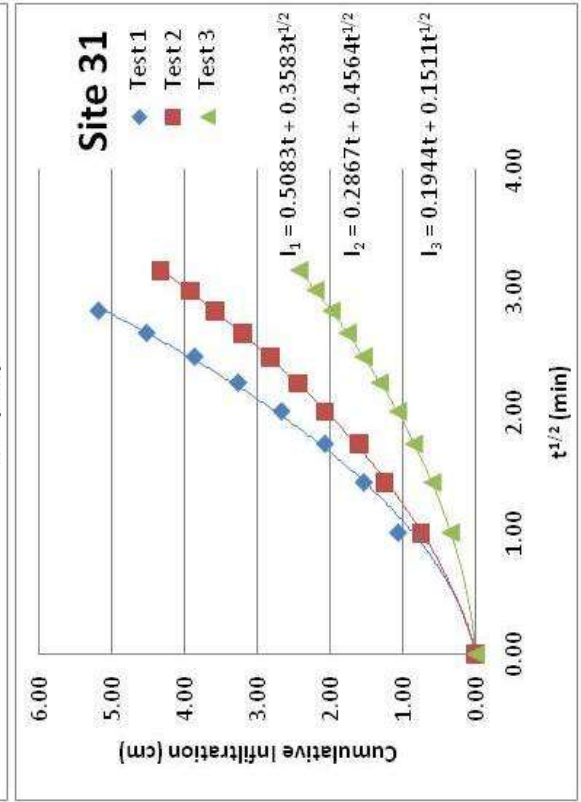
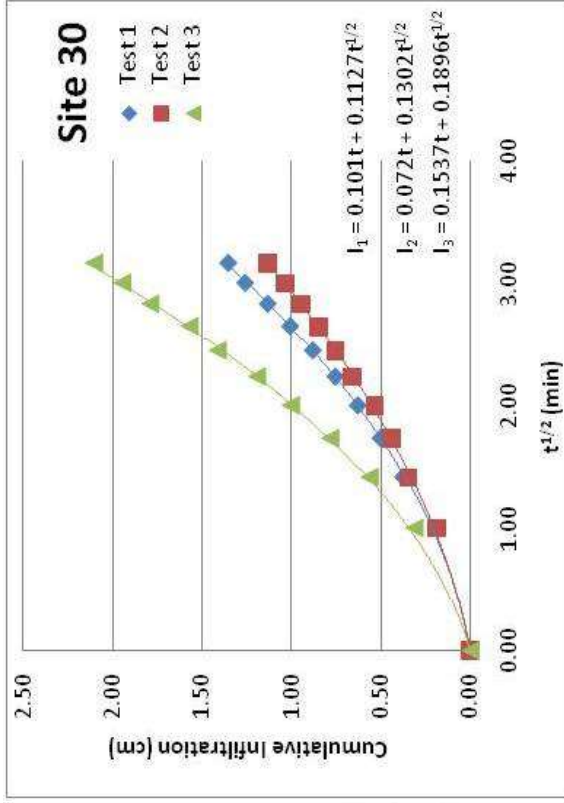
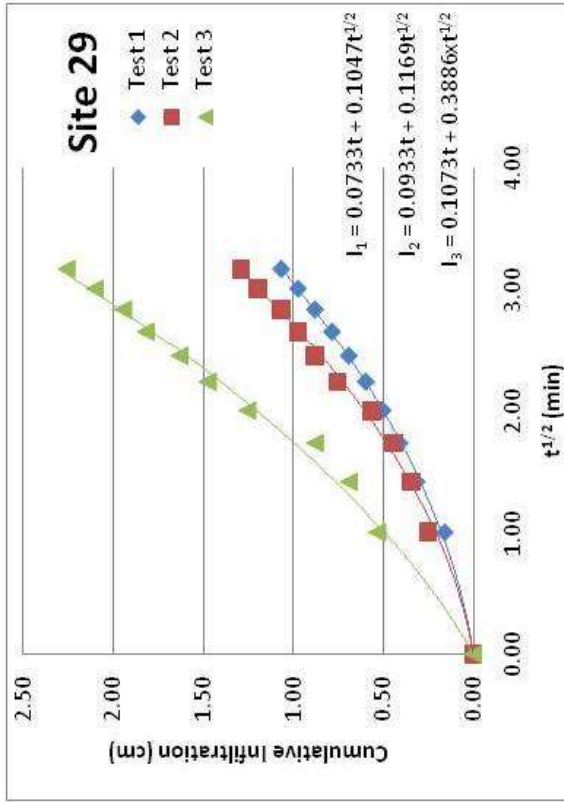












APPENDIX B

This appendix contains results from the double-ring infiltrometer tests. Each test corresponds to a measurement location shown in Figure 4.1. As noted in chapter 4.1.2.2, hydraulic conductivity was determined from the late time data as the infiltration rate approaches a constant value.

